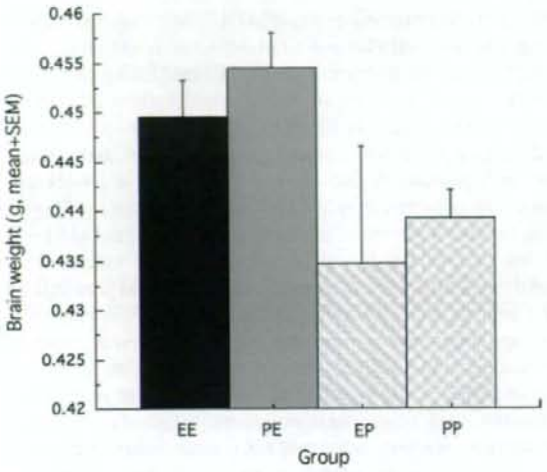


Fig. 6. Brain weight of four groups of mice. Brain was removed and weighted at the next day of the passive avoidance test (13 weeks old) (mean + S.E.M.).

Fig. 8 shows numbers of neurons stained for BrdU in hippocampus (A) and cerebral cortex (B). Neurons were counted in 10 sections for each animal, and were averaged. ANOVA including data for the hippocampus indicated the effect of group to be significant [$F(3, 24) = 8.516$, $p = .0005$]. Post hoc tests showed that group differences between EE and EP, EE and PP, EP and PE, and PE and PP were significant. Thus, environmental enrichment benefited generation of hippocampal neurons, with the most recent environment being critical. PE mice produced more new neurons in the hippocampus than EP mice. Next, ANOVA including data of the cerebral cortex also indicated that the effect of group was significant [$F(3, 25) = 3.169$, $p = .0418$]. Post hoc tests suggested that group differences between EE and EP, EP and PE, and EP and PP groups were significant.

Neurons thus began to increase significantly within 2 weeks after beginning of exposure to the enriched condition. Even a short period of enrichment augmented neuronal proliferation.

## 4. Discussion

Results of the present experiments reconfirmed that environmental enrichment between weaning and adult had affected development and function of the mouse brain. The brain was

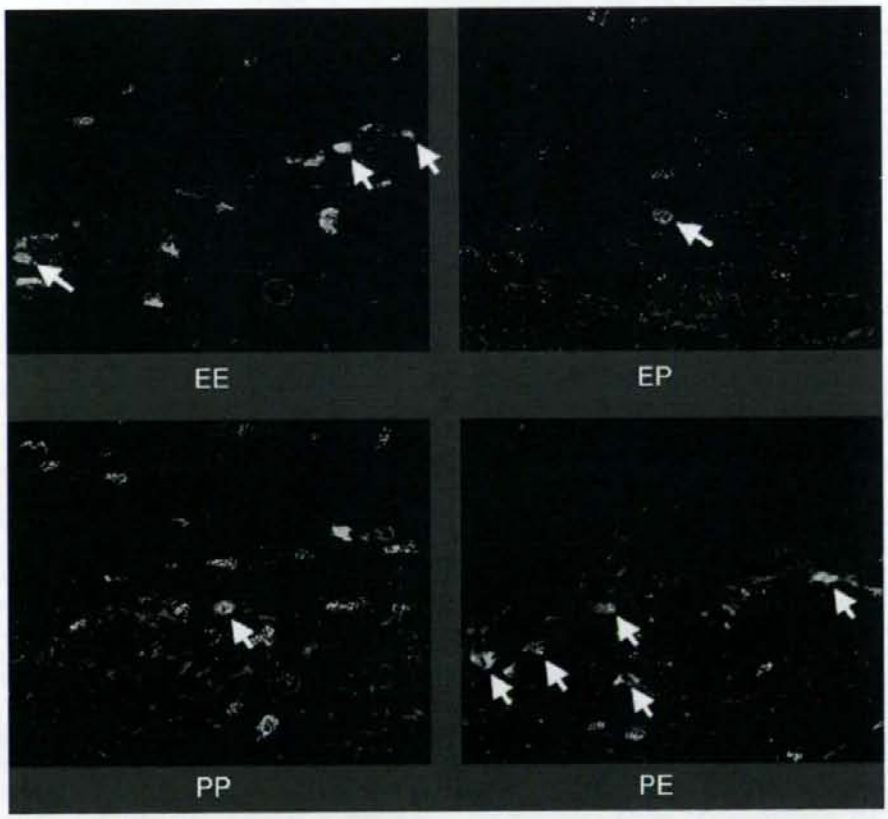


Fig. 7. Newly generated neurons in the hippocampus (arrows). Sections were visualized by confocal microscopy with antibody labeling for BrdU and PSA-NCAM. One example is presented for each group. Original magnification: 200×.

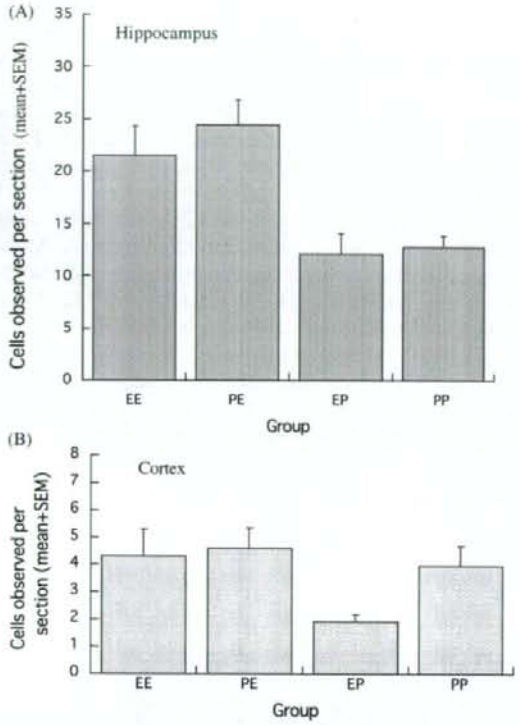


Fig. 8. Newly generated neurons in hippocampus (A) and cerebral cortex (B) per section (mean + S.E.M.). The two groups experienced enrichment during last 2 weeks (EE, PE) showed significantly more neurons labeled by BrdU than the two groups experienced impoverishment during last 2 weeks (EP, PP) in hippocampus. Group EP generated new neurons significantly less than the other three groups in cortex.

heavier in the EE group than the PP group, as in early studies [38,40]. Greater locomotive activities of the PP animals in the open-field test [10,33,41] and smaller prepulse inhibition in the PP mice than EE animals [6] were same as results reported in previous studies. Superior learning in EE mice compared with PP animals also agreed with results of earlier studies [11,29,50].

Moreover, results in the two environment exchange groups indicated that the effect of environment was determined by the most recent condition, suggesting that the plasticity or reorganisation of the brain could take place within a few weeks, even in adult mice. Behavioural results for PE mice resembled to the EE in open-field activity, startle amplitude, water-maze performance, and the probe test; brain weight also was greatest. Some researchers have reported that early impoverishment induced severe and irreversible deficiency in the rats' brain [9,13,51]. Or, development of the brain was not altered by impoverishment, once rats had experienced enrichment [19]. Our results of mice disagreed, the PE group, exposed to an impoverished environment in early life showed superior behavioural performance and heavier brains than the EP group exposed to an enriched environment during early life.

Indirect evidence has accumulated suggesting nervous tissue generation during enrichment [22,23,29,30], an effect also reported after running exercise [47,48]. We therefore expected that neurons would be generated during enriched experience in adult animals even over a short period. Indeed, long-term enrichment was found to increase hippocampal neurons in adult mice [20,21]. Our results in the PE and EP groups were critical in addressing this issue. The PE group generated many neurons in the hippocampus and cerebral cortex after a 2-week experience of enrichment, while results in the EP group suggested the beneficial effects of enrichment early in life could be nullified by impoverishment of conditions for 2 weeks, even in adult mice. Behavioural measures agreed with the anatomic data. PE mice performed better than EP animals, resembling the EE group. The present results that even a short period of enrichment promoted nerve cell generation with behavioural improvement, while a short period of impoverishment induced poor anatomic and behavioural outcomes, suggested that housing conditions are very important for reliable behavioural evaluation of experimental animals. Even "knockedout" mice missing a neurologically important gene reportedly recovered learning and memory after enrichment [8,35]. The results in this area of researches are almost always put in the context of enrichment [20,21,29,38–40]. However, the present results of the EP and PE groups suggest that it is important to study the effects of impoverishment as equally as enrichment. Standardization of housing conditions thus may be unexpectedly important in behavioural neuroscience.

We developed a speculative hypothesis concerning neuronal generation during enriched housing. After observing animals' behaviour in their home cages, enriched and impoverished animals lived completely differently. Enriched animals showed many types of movement, including running, chasing, crouching and fighting, hiding, climbing and wheel-running, and established social order among cage mates. These activities might activate neurons in specific areas of the brain such as hippocampus, cerebral cortex, hypothalamus, visual and motor areas and cerebellum. On the other hand, impoverished mice seldom moved, with less brain activation as a likely consequence. Activation of neurons could induce neurochemical excitation with an increase in regional cerebral blood flow as shown by functional magnetic resonance imaging (fMRI). Recent findings have shown neuronal regeneration after cerebral ischemia [3,28], regeneration was promoted if blood flow in ischemic brain was restored by angiogenesis [45]. Mechanisms underlying such effects are unclear, but recovery of blood flow might accelerate removal of debris or toxic products from the injured brain, and/or enhance production of chemokines and trophic agents [23,30]. If this hypothesis is true, neuron genesis and functional enhancement by enrichment in young adult mice might arise from brain stimulation and remodeling of blood flow. Our findings showed that an enriched environment enhanced neuron genesis in the mouse hippocampus and cingulated cortex, both of which participate in memory function. On the other hand, impoverished environment impaired neuron genesis. Based on these data, enriched experience appears to be essential for enhancing endogenous neuron genesis and improving functional recovery.

Recent animal welfare movement has advocated important of housing and care for laboratory rodents, giving animals greater

opportunity to carry out species-specific behavioural repertoires [4,18]. To answer the demand for standardized of environmental enrichment for laboratory animals, increasing numbers of rodent care products are coming available, even accommodating differences in preference for nest boxes in mice [46]. Improvements in housing conditions are expected to cause some discrepancies between early and present data, not only in behavioural observations but also for other biologic characteristics.

Finally, environmental enrichment has been used to promote the mental health of persons at risk [36,37]. For example, Rane et al. [36] assessed the effect of environmental enrichment including nutrition, education, and physical exercise at ages from 3 to 5 years in children with risk factors for later emergence of schizophrenia. Schizotypical personality features and antisocial behaviour were assessed at the ages of 17 and 23 years. Results suggested that the early enrichment program was effective; subjects who participated had more normal scores upon assessment in adolescence than untreated at-risk controls. These results are consistent with animal studies in which an enriched environment benefited behavioural and biologic outcomes. Moreover, our finding that even a short period of environmental enrichment positively affected behaviour and generation of neurons in the adult mouse suggested that even adults and elderly persons could benefit from enrichment, improving cognitive and memory functions. On the other hand, hospitalization or isolation might cause deterioration even in adults. Although the present experiment could not differentiate physical and social environments as the factor to influence the present results, we would like to testify whether social or physical, or the combination of both factors, cause the present effects in the future study.

## Acknowledgments

This work was partially supported by a Grant-in Aid for Scientific Research (C) No. 17530540 in the Japanese Ministry of Education, Science, Sports and Culture and by a Research Grant for Cardiovascular Diseases. We would like to thank Ms. Yuka Okinaka for technical assistance.

## References

[1] Akita H, Matsuyama T, Iso H, Sugita M, Yoshida S. Effects of oxidative stress on the expression of limbic-specific protease neuropsin and avoidance learning in mice. Brain Res 1997;967:86–96.
[2] Altman JA, Das GD. Autoradiographic examination of the effects of enriched environment on the rate of glial multiplication in the adult rat brain. Nature 1964:1161–3.
[3] Arvidsson A, Collin T, Kirik D, Kokaia Z, Lindvall O. Neuronal replacement from endogenous precursors in the adult brain after stroke. Nat Med 2002;8:963–70.
[4] Baumans V. Environmental enrichment for laboratory rodents and rabbits: requirements of rodents, rabbits, and research. ILAR J 2005;46:162–70.
[5] Benaroya-Milshtein N, Hollander N, Apter A, Kukulansky T, Raz N, Wilf A, et al. Environmental enrichment in mice decreases anxiety, attenuates stress responses and enhances natural killer cell activity. Eur J Neurosci 2004;20:1341–7.
[6] Cilia J, Reavill C, Hagan JJ, Jones DNC. Long-term evaluation of isolation-rearing induced prepulse inhibition deficits in rats. Psychopharmacology 2001;156:327–37.
[7] Dannis C. All in the mind of a mouse. Nature 2005;438:151–2.
[8] Duffy SN, Craddock KJ, Abel T, Nguyen PV. Environmental enrichment modifies the PKA-dependence of hippocampal LTP and improves hippocampus-dependent memory. Learn Memory 2001;8:26–34.
[9] Einon DF, Morgan MJ. A critical period for social isolation in the rat. Dev Psychobiol 1977;10:123–32.
[10] Elliott BM, Grunberg NE. Effects of social and physical enrichment on open field activity differ in male and female Sprague–Dawley rats. Behav Brain Res 2005;165:187–96.
[11] Ferchmin PA, Eterovic VA. Forty minutes of experience increase the weight and RNA content of cerebral cortex in periadolescent rats. Dev Psychobiol 1986;19:511–9.
[12] Ferchmin PA, Eterovic VA, Caputto R. Studies of brain weight and RNA content after short periods of exposure to environmental complexity. Brain Res 1970;20:49–57.
[13] File SE. Exploration, distraction, and habituation in rats reared in isolation. Dev Psychobiol 1978;11:73–81.
[14] Gentch C, Lichtsteiner M, Frischnecht HR, Feer H, Siegfried B. Isolation-induced locomotor hyper-activity and hypoanalgesia in rats are prevented by handling and reversed by resocialisation. Physiol Behav 1988;43:13–6.
[15] Gobbo OL, O'Mara SM. Impact of enriched-environment housing on brain-derived neurotrophic factor and on cognitive performance after a transient global ischemia. Behav Brain Res 2004;152:231–41.
[16] Gottleb G, Blair C. How early experience matters in intellectual development in the case of poverty. Prevent Sci 2004;5:245–52.
[17] Huck UW, Price EO. Differential effects of environmental enrichment on the open-field behavior of wild and domestic Norway rats. J Comp Physiol Psychol 1975;89:892–8.
[18] Hutchinson E, Avery A, Vandewoude S. Environmental enrichment for laboratory rodents. ILAR J 2005;46:148–61.
[19] Katz HB, Davies CA. Effects of differential environments on the cerebral anatomy of rats as a function of previous and subsequent housing conditions. Exp Neurol 1984;83:274–87.
[20] Kempermann G, Brandon EP, Gage FH. Environmental stimulation of 129/SvJ mice causes increased cell proliferation and neurogenesis in the adult dentate gyrus. Curr Biol 1998.
[21] Kempermann G, Kuhn HG, Gage FH. More hippocampal neurons in adult mice living in an enriched environment. Nature 1997;386:493–5.
[22] Leggio MG, Mandolesi L, Federico F, Spirito F, Ricci B, Gelfo F, et al. Environmental enrichment promotes improved spatial abilities and enhanced dendritic growth in the rat. Behav Brain Res 2005;163:78–90.
[23] Lewis MH. Environmental complexity and central nervous system development and function. Mental Retard Dev Disabil Rev 2004;10:91–5.
[24] Lodge DJ, Lawrence AJ. The effect of isolation rearing on volitional ethanol consumption and central CCK/dopamine systems in Fawn-Hooded rats. Behav Brain Res 2003;141:113–22.
[25] Matsuyama S, Doe N, Kurihara N, Tanizawa K, Kuroda S, Iso H, et al. Spatial learning of mice lacking a neuron-specific epidermal growth factor family protein, NELL2. J Pharmacol Sci 2005;98:239–43.
[26] McIlwain KL, Merriweather MY, Yuva-Paylor LA, Paylor R. The use of behavioral test batteries: effects of training history. Physiol Behav 2001;73:705–17.
[27] Morgan MJ. Effects of post-weaning environment on learning in the rat. Anim Behav 1973;21:429–42.
[28] Nakatomi H, Kuriu T, Okabe S, Yamamoto S, Hatano O, Kawahara N, et al. Regeneration of hippocampal pyramidal neurons after ischemic brain injury by recruitment of endogenous neural progenitors. Cell 2002;110:429–41.
[29] Pham TM, Soderstrom S, Winblad B, Mohammed AH. Effects of environmental enrichment on cognitive function and hippocampal NGF in the non-handled rats. Behav Brain Res 1999;103:63–70.
[30] Pham TM, Winblad B, Granholm A, Mohammed AH. Environmental influences on brain neurotrophines in rats. Pharmacol Biochem Behav 2002;73:167–75.
[31] Phillips GD, Howes SR, Whitelaw RB, Robbins TW, Everitt BJ. Isolation rearing impairs the reinforcing efficacy of intravenous cocaine or intra-accumbens D-amphetamine: impaired response to intra-accumbens D1 and D2/D3 dopamine receptor antagonists. Psychopharmacology 1994;115:419–29.

[32] Phillips GD, Howes SR, Whitelaw RB, Wilkinson LS, Robbins TW, Everitt BJ. Isolation rearing enhances the locomotor response to cocaine and a novel environment, but impairs the intravenous self-administration of cocaine. Psychopharmacology 1994;115:407–18.
[33] Pietropaolo S, Branchi I, Cirulli F, Chiarotti F, Aloe L, Alleva E. Long-term effects of the periadolescent environment on exploratory activity and aggressive behaviour in mice: social versus physical enrichment. Physiol Behav 2004;81:443–53.
[34] Pryce CR, Bettschen D, Nanz-Bahr NI, Feldon J. Comparison of the effects of early handling and early deprivation on conditioned stimulus, context, and spatial learning and memory in adult rats. Behav Neurosci 2003;117:883–93.
[35] Rampon C, Tang Ya-P, Goodhouse J, Shimizu E, Kyin M, Tsien JZ. Enrichment induces structural changes and recovery from nonspatial memory deficit in CA1 NMDAR1-knockout mice. Nat Neurosci 2000;3:238–45.
[36] Rane A, Mellingen K, Liu J, Vanables PH, Mednick SA. Effects of environmental enrichment at ages 3–5 years on schizotypical personality and antisocial behavior at ages 17 and 23 years. Am J Psychiatry 2003;160:1627–35.
[37] Rane A, Vanables PH, Dalais C, Mellingen K, Reynolds C, Mednick SA. Early educational and health enrichment at age 3–5 years is associated with increased autonomic and central nervous system arousal and orienting at age 11 years: evidence from Mauritius Child Health Project. Psychophysiology 2001;38:254–66.
[38] Rosenzweig MR. Environmental complexity, cerebral change, and behavior. Am Psychol 1966;21:321–32.
[39] Rosenzweig MR, Bennett EL. Psychobiology of plasticity: effects of training and experience on brain and behavior. Behav Brain Res 1996;78:57–65.
[40] Rosenzweig MR, Krech D, Bennett EL, Diamond MC. Effects of environmental complexity and training on brain chemistry and anatomy: a replication and extension. J Comp Physiol Psychol 1962;55:429–37.
[41] Sahakian BJ, Robbins TW, Morgan MJ, Iversen SD. The effects of psychomotor stimulants on stereotypy and locomotor activity in socially-deprived and control rats. Brain Res 1975;84:195–205.
[42] Sasaki H, Iso H, Coffey P, Inoue T, Fukuda Y. Prepulse facilitation of auditory startle response in hamsters. Neurosci Lett 1998;248:117–20.
[43] Seki T, Arai Y. The persistent expression of a highly polysialylated NCAM in the dentate gyrus of the adult rat. Neurosci Res 1991;12:503–13.
[44] Seki T, Arai Y. Highly polysialylated neural cell adhesion molecule (NCAM) is expressed by newly generated granule cells in the dentate gyrus of the adult rat. J Neurosci 1993;13:2351–8.
[45] Taguchi A, Soma T, Tanaka H, Kanda T, Nishimura H, Yoshikawa H, et al. Administration of CD34+ cells after stroke enhances neurogenesis via angiogenesis in a mouse model. J Clin Invest 2004;114:330–8.
[46] Van Loo PL, Bloom HJ, Meijer MK, Baumans V. Assessment of the use of two commercially available environmental enrichments by laboratory mice by preference testing. Lab Anim 2005;39:58–67.
[47] Van Praag H, Cristie BR, Sejnowski TJ, Gage FH. Running enhances neurogenesis, learning and long-term potentiation in mice. Proc Natl Acad Sci USA 1999;96:13427–31.
[48] Van Praag H, Kempermann G, Gage FH. Running increases cell proliferation and neurogenesis in the adult mouse dentate gyrus. Nat Neurosci 1999;2:266–70.
[49] Van Praag H, Kempermann G, Gage FH. Neural consequences of environmental enrichment. Nat Rev Neurosci 2000;1:191–8.
[50] Wood WE, Greenough WT. Effect of grouping and crowding on learning in isolation-reared adult rats. Bull Psychon Soc 1974;3:65–7.
[51] Wright IK, Upton N, Marsden CA. Resocialization of isolation-reared rats does not alter their anxiogenic profile on the elevated X-maze model of anxiety. Physiol Behav 1991;50:1129–32.
[52] Yukawa K, Iso H, Tanaka T, Tsubota Y, Owada-Makabe K, Bai T, et al. Down-regulation of dopamine transporter and abnormal behavior in STAT6-deficient mice. Int J Mol Med 2005;15:819–25.
[53] Yukawa K, Tanaka T, Owada-Makabe K, Tsubota Y, Bai T, Maeda M, et al. Reduced prepulse inhibition of startle in STAT6-deficient mice. Int J Mol Med 2005;16:673–5.

Available online at www.sciencedirect.com
ScienceDirect
Neuroscience Letters xxx (2007) xxx–xxx
Neuroscience Letters
www.elsevier.com/locate/neulet

# Sema4D-plexin-B1 implicated in regulation of dendritic spine density through RhoA/ROCK pathway

Xianzong Lin[a,b], Mariko Ogiya[b], Mizue Takahara[b], Wataru Yamaguchi[b], Tatsuo Furuyama[b,c], Hidekazu Tanaka[d], Masaya Tohyama[a], Shinobu Inagaki[b,*]

[a] Department of Anatomy and Neuroscience, Osaka University Graduate School of Medicine, Yamadaoka 2-2, Suita, Osaka 565-0871, Japan
[b] Group of Neurobiology, Division of Health Sciences, Osaka University Graduate School of Medicine, Yamadaoka 1-7, Suita, Osaka 565-0871, Japan
[c] Department of Nutrition, School of Human Health, Sonoda Women's University, Amagasaki, Hyogo 661-8520, Japan
[d] Department of Pharmacology, Osaka University Graduate School of Medicine, Yamadaoka 2-2, Suita, Osaka 565-0871, Japan

Received 23 July 2007; received in revised form 2 September 2007; accepted 19 September 2007

**Abstract**

Plexin-B1, Sema4D receptor, mediates retraction and extension signals in axon guidance by associating with PDZ-containing Rho guanine nucleotide exchange factors (PDZ-RhoGEFs) which can activate a small Rho GTPase RhoA. RhoA is implicated in spine formation by rearranging actin cytoskeleton. Exogenous application of Sema4D to cultured neurons caused activation of RhoA, increase of spine density and changes in spine shape. Sema4D-induced changes in spine density were blocked by either Rho-kinase (a downstream of RhoA, ROCK) inhibitor Y-27632 or by overexpression of plexin-B1 mutant lacking the C-terminus which no longer associates with PDZ-RhoGEFs. This study suggests that Sema4D-plexin-B1 play a crucial role in spine formation by regulating RhoA/ROCK pathway.
© 2007 Elsevier Ireland Ltd. All rights reserved.

*Keywords:* Semaphorin; Plexin; Rho; Dendritic spine; Cytoskeleton; Neuron

Semaphorins comprise a family of soluble and transmembrane proteins that play a critical role in axon guidance in the developing nervous system [16,18,32]. Semaphorins trigger dynamic rearrangements of actin cytoskeleton and induce retraction or extension of neurites [3,17,19,20,25,28]. Expressions of several semaphorins and their functional receptors, plexins, persist into adulthood after axon guidance has been completed [10,15,19–21,33,36]. However, roles of semaphorins at postnatal ages are not well understood.

Dendritic spines, actin-rich protrusions on neuronal dendrites, are the major postsynaptic sites of excitatory synapses in the brain [7,11–13]. The spine formation and morphology are regulated by reorganizing actin cytoskeleton [4,12]. Rho GTPases, RhoA, Rac and Cdc42 are important in this regulation [22,34]. They are active when bound to GTP and inactive when bound to GDP, act as intracellular molecular switches and transduce signals from extracellular stimuli to the actin cytoskeleton. However, little is known about external cues that trigger the activation of Rho GTPases in spine formation and morphogenesis. Sema4D is such a candidate, because it and its receptor plexin-B1 are highly expressed in the brain during early postnatal period the synaptic formation stage [9,36], and mediate RhoA-signaling via direct association with PDZ (postsynaptic density-95/Discs large/zona occludens-1) domain-containing Rho guanine nucleotide exchange factors (PDZ- RhoGEFs) (positive regulators of RhoA activation), p190-Rho guanine nucleotide activating protein (RhoGAP) (a negative regulator of RhoA-signaling), and a RhoGTPase Rnd1 [3,13,23,26,33]. Here, we investigate whether Sema4D-plexin-B1 is involved in spine formation and morphogenesis of cultured hippocampal neurons via RhoA/Rho-kinase (ROCK) pathway.

Hippocampal neurons were cultured as described by Banker and Goslin [2] with modifications. In brief, the hippocampal tissues were dissociated from Sprague-Dawley rat embryos of embryonic day 18 (E18) (SLC), and digested in 10 ml of 4 U/ml papain (Worthington Biochem)/0.0015% DNase (Sigma)/0.02 M phosphate buffered saline (PBS)/0.2 mg/ml DL-cysteine HCl/0.2 mg/ml bovine serum albumin (BSA) (Sigma)/5 mg/ml glucose in 50 ml tube for 15 min at 37 °C.

* Corresponding author. Tel.: +81 6 6879 2581; fax: +81 6 6879 2581/2629.
*E-mail address:* inagaki@sahs.med.osaka-u.ac.jp (S. Inagaki).

0304-3940/$ – see front matter © 2007 Elsevier Ireland Ltd. All rights reserved.
doi:10.1016/j.neulet.2007.09.045

Please cite this article in press as: X. Lin, et al., Sema4D-plexin-B1 implicated in regulation of dendritic spine density through RhoA/ROCK pathway, Neurosci. Lett. (2007), doi:10.1016/j.neulet.2007.09.045

Suspended neurons were plated at 150 cells/mm$^2$ onto coverslips (Matsunami Glass), which were coated overnight with 2 mg/ml poly-L-lysine (Sigma) in 0.15 M borate buffer (pH 8.4). Neurons were cultured in Neurobasal medium (GIBCO)/B27 (GIBCO) and 25 μM L-glutamine. Two days after plating, the medium was exchanged with fresh Neurobasal/B27 every 3 days, and after 7 day-in vitro (DIV) one half of the medium was exchanged. Hippocampal neurons were transfected at 5-DIV with green fluorescent protein (GFP, Clonetech) together with or without a deletion mutant of plexin-B1ΔC (plexin-B1 lacking C-terminal three amino acids) by the calcium phosphate method as described [2,13]. Neurons were usually analyzed at 21-DIV.

Human embryonic kidney (HEK293) cells were cultured with 10% fetal bovine serum (FBS, Race, Australia)/Dulbecco's modified Eagle's medium (DMEM), and transfected with HA-tagged-human plexin-B1 (KIAA0407) [13], human plexin-B2 (KIAA0315) [13], and mouse plexin-A1 [15], and the cells were subjected to Western blot analysis. Sema4D-Fc (Fc-tagged extracellular region of mouse Sema4D) was obtained as described previously [8,9], and used as soluble Sema4D.

Polyclonal antibodies to plexin-B1 were raised by immunizing rabbits with maltose binding protein (MBP)-fused-mouse plexin-B1 (amino acid, 1216–1521, NM_17725). The specificity of the antibodies was confirmed by Western blot analysis. Mouse monoclonal antibody to HA was obtained from Boehringer–Mannheim, antibody to postsynaptic density protein (PSD-95) from Upstate Biotechnology and antibody to RhoA from Santa Cruz [13,14,37]. For Western blot analysis, primary antibodies were used at a dilution of 1:2000 (anti-plexin-B1, RhoA) and 1:10,000 (anti-HA), and for immunocytochemistry, anti-PSD-95 and anti-plexin-B1 were used at 1:500.

For Western blot analysis, cells were lysed in ice-cold lysis buffer (20 mM Tris–HCl pH 7.5, 1 mM EDTA–Na, 150 mM NaCl, 1% TritionX-100, 1 mM phenyl-methylsulfonyl fluoride (PMSF)), left on ice for 30 min, and the supernatant was pro-

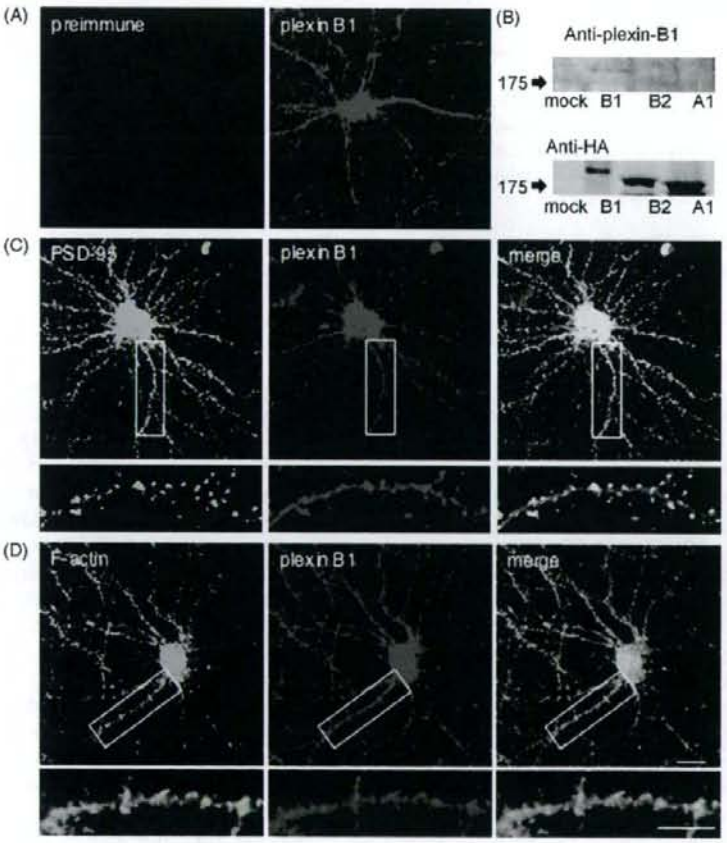


Fig. 1. Immunostaining for plexin-B1 in dendrites of cultured hippocampal neurons. (A) Cultured hippocampal neurons (21-DIV) were stained with the preimmune or the polyclonal antiserum to plexin-B1. (B) Western blot analysis shows the characteristics of the antiserum to plexin-B1. The antibodies recognize HA-tagged plexin-B1 (B1) but not plexin-B2 (B2) or plexin-A1 (A1) transfected in HEK 293 cells. (C and D) Immunofluorescent images of 21-DIV hippocampal neurons show localization of PSD-95 (green) and plexin-B1 (red) (C), and that of F-actin stained with FITC-phalloidin and plexin-B1 (red) (D). These images show colocalization of plexin-B1 with PSD-95 and with F-actin in dendritic spines. Scales: 10 μm (upper panels), 20 μm (lower panels). (For interpretation of the references to color in this figure legend, the reader is referred to the web version of the article.)

Please cite this article in press as: X. Lin, et al., Sema4D-plexin-B1 implicated in regulation of dendritic spine density through RhoA/ROCK pathway, Neurosci. Lett. (2007), doi:10.1016/j.neulet.2007.09.045

ceeded for SDS-PAGE electrophoresis and Western blot analysis as described previously [13]. The membrane was treated with 5% skim-milk/Tris–HCl (pH 7.5), incubated with primary antibody for 1 h, washed three times in 0.5% Tween 20/Tris–HCl, incubated with HRP-labeled secondary antibody (1:10,000) (Jackson Immunoresearch), and finally visualized by enhanced chemiluminescence ECL (Amersham).

Immunocytochemical staining was performed as described with modifications [14]. 21-DIV cultured hippocampal neurons and other cells were fixed in 10% formalin/PBS for 30 min, permeabilized with 0.25%Triton X-100/PBS for 10 min, washed in PBS twice, blocked in 10% BSA/PBS for 60 min, and then incubated with indicated primary antibodies in 3% BSA/PBS for 4 h at room temperature. After washed in PBS, cells were incubated for 2 h with Cy3- (1:2000) or FITC- (1:500) labeled goat anti-mouse or anti-rabbit-IgG (Jackson Immunoresearch), and/or FITC- (1:500) or TRIC-labeled phalloidin (1:1000) (Sigma). Neurons on coverslips washed in PBS were mounted in 95% glycerol on glass slides.

Serial confocal images of neurons were obtained with the LSM 510 confocal imaging system (Zeiss) using an oil immersion, 63× objective with sequential-acquisition as described previously [1,5,30]. Serial optical sections were taken at an interval of 0.5 μm for each image with 3× zoom. For measurement of spine density and morphology, spines located in the proximal 100-μm segments of the largest two dendrites were chosen from GFP-positive neurons, and manually traced. Then spine density and length were counted or measured automatically with LSM510 software (Zeiss). For each experimental group, more than 10 transfected neurons were chosen randomly for quantification from 3–4 coverslips derived from three independent experiments, and at least 200 spines were counted from more than 10 neurons visualized by GFP fluorescence as described elsewhere [5,30]. Spines were defined as described by Harris et al. [11]. Measured data were exported to Excel software (Microsoft), and the data were compared with Student's *t*-test. At least three independent experiments were performed for each experiment. Statistical significance was determined ($p < 0.01$) using Student's *t*-test.

Detection of active RhoA was performed as described previously [37]. Cultured neural cells ($1 \times 10^7$ cells) prepared from cerebral cortex containing hippocampus were lysed in ice-cold lysis buffer (50 mM Tris–HCl, pH 7.5, 100 mM NaCl, 10 mM $MgCl_2$, 10% glycerol, 1% Triton X-100, 1 mM PMSF). The supernatant was incubated with 16 μg of GST-rhotekin Rho-binding domain [29]. The bound RhoA was eluted by boiling in sample buffer for SDS-PAGE and subjected to Western blot analysis with anti-RhoA antibody.

To verify the expression of plexin-B1 in dendrites, primary cultured hippocampal neurons were immunostained with anti-plexin-B1 antibodies. Plexin-B1 immunoreactivity was seen in the neuronal cell bodies, dendrites and dendritic spines, while no specific immunostaining was found in the control sections immunostained with the preimmune serum (Fig. 1A). Western blot analysis showed that the antibody reacts with plexin-B1 overexpressed in HEK293 cells, while does not with plexin-

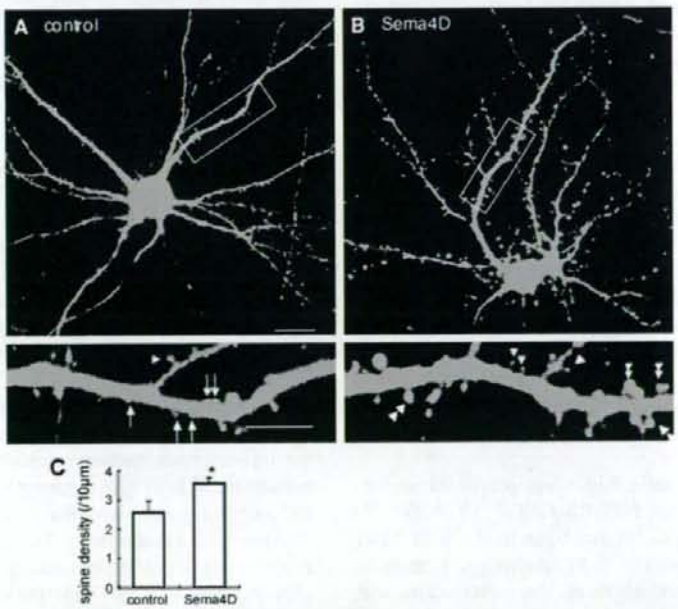


Fig. 2. Effects of Sema4D on dendritic spines. (A and B) Confocal GFP-images for dendritic morphology of cultured hippocampal neurons (21-DIV). Neurons transfected with GFP were untreated (A) or treated with 1 nM Sema4D-Fc for 6 h (B). Scales: 10 μm (upper panels), 20 μm (lower panels). Examples of stubby, thin and mushroom spines are indicated by arrows, arrowheads and double-arrowheads, respectively. (C) Spine density (per 10 μm-segment) was quantified in the proximal 100-μm-segments of the two largest dendrites from 15 neurons. Treatment of hippocampal neurons with Sema4D-Fc increased spine density. Data represent the mean spine density ± S.D. ($n = 15$ neurons per group), $^*p < 0.001$ with Student *t*-test.

Please cite this article in press as: X. Lin, et al., Sema4D-plexin-B1 implicated in regulation of dendritic spine density through RhoA/ROCK pathway, Neurosci. Lett. (2007), doi:10.1016/j.neulet.2007.09.045

B2 or plexin-A1 (Fig. 1B). Focusing on dendrites and dendritic spines, immunostaining for plexin-B1 was present in dendritic shafts and in punctuate structures along the shaft of hippocampal neurons. Dots-like plexin-B1-stainings were colocalized with PSD-95 (Fig. 1C), and also with F-actin (Fig. 1D). Our data show that plexin-B1 is endogenously expressed in dendritic spines and shafts.

In addition to the expression of plexin-B1 in dendrites, its ligand Sema4D is expressed in postnatal and adult brains [9,36]. To determine whether Sema4D-plexin-B1 contribute to spine formation we examined the effects of Sema4D on density of dendritic spines in cultured hippocampal neurons visualized by a transient transfection with GFP. Application of soluble Sema4D led to a significant increase of spine density (Fig. 2). The average density of dendritic spines was $2.58 \pm 0.39$ (per 10-μm) in control neurons treated with the control medium, while it was $3.56 \pm 0.19$ in neurons treated with the Sema4D-containing medium. Treatment with Sema4D had no significant affect on the length of spines (control, $0.93 \pm 0.14$ μm; Sema4D, $1.04 \pm 0.09$). Spine morphology is matured during development in the order of stubby, thin, and mushroom-types [6,11]. Stubby spines predominate in control 21-DIV hippocampal neurons, while thin and mushroom spines become predominant following treatment with Sema4D (Fig. 2). Taken together, our findings suggest that Sema4D promotes spine formation and morphological maturation of spines.

The effects of Sema4D on neurons are known to be mediated by plexin-B1 and its downstream signaling that is engaged in regulation of RhoA [13,26,33]. Sema4D-effect on RhoA was examined in whole cell lysates of neuron-rich culture from the cerebral cortex containing the hippocampus. Treatment with Sema4D induced activation of RhoA in cultured neurons (Fig. 3A). We therefore examined whether a major downstream effector of RhoA ROCK is involved in Sema4D-induced spine formation, using Y-27632, a specific ROCK inhibitor [35]. Treatment of hippocampal neurons with Y-27632 significantly reduced spine density (control, $2.48 \pm 0.17$/10 μm; Y27632, $1.72 \pm 0.24$) and eliminated Sema4D-induced increase in spine density (Sema4D, $3.57 \pm 0.09$/10 μm; Sema4D + Y-27632, $1.50 \pm 0.16$) (Fig. 3B and C). Simultaneous application of Y-27632 and Sema4D almost completely blocked Sema4D-induced increase in spine density. As previously described [27,34], Y-27632 increased the length of spines, while Y-27632 had no such effect when neurons were simultaneously treated with Sema4D (data not shown). These results suggest that RhoA/ROCK pathway is implicated in Sema4D-induced spine formation.

Sema4D can enhance active RhoA via plexin-B1 and its C-terminal association with PDZ-RhoGEFs [13,26,33]. To investigate whether the association of plexin-B1 with PDZ-RhoGEFs is required for Sema4D-induced changes in dendritic spines, plexin-B1ΔC mutant, which no longer associates with PDZ-RhoGEFs, was introduced into cultured hippocampal neurons. Transfection with plexin-B1ΔC completely blocked Sema4D-induced elevation of spine density (Fig. 4), while transfection with wild type-plexin-B1 did not block such Sema4D-induced elevation (data not shown).

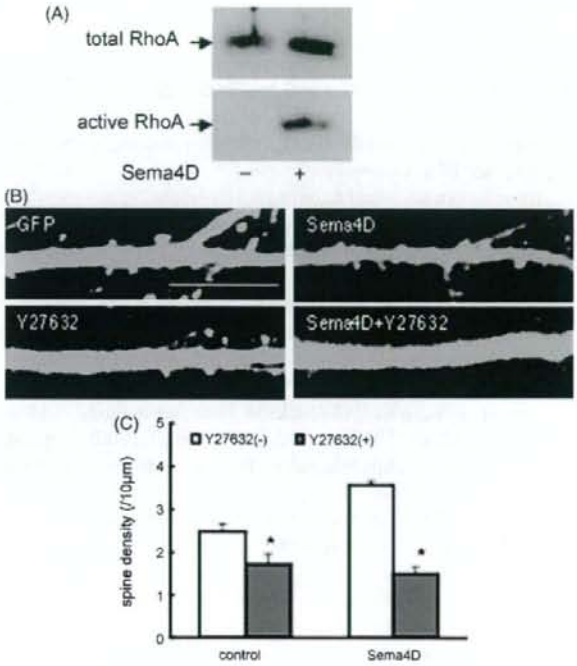


Fig. 3. Effects of Sema4D on neurons and blockade of ROCK. (A) Cultured cortical neurons (9-DIV) treated with or without 1 nM of Sema4D-Fc for 30 min. The lysates were incubated with GST-rhotekin beads. Bound active RhoA was subjected to SDS-PAGE followed by Western blot analysis with the anti-RhoA antibody. (B) Confocal GFP images show examples of dendritic spines of 21-DIV hippocampal neurons transfected with GFP. Neurons pretreated with or without 10 μM Y-27632, a ROCK inhibitor, were treated with or without 1 nM Sema4D-Fc for 6 h. Scale: 20 μm. (C) The effects of Y-27632 on spine density (per 10 μm-segment) were quantified from 15 neurons (two dendrites per neuron). Data represent the mean ± S.D. $*p < 0.001$ with Student $t$-test.

Plexin-B1 is widely found in the brain, and distributed in neuropils as well as over neuronal cell bodies in the hippocampus [33]. In this study, the immunostaining for plexin-B1 was confirmed in dendrites and dendritic spines, and it was colocalized with PSD-95, suggesting that plexin-B1can function as the receptor for Sema4D at dendrites and dendritic spines. The present data show that Sema4D plays a crucial role in regulating the spine density and morphology. Application of exogenous Sema4D increased the spine density, and thin and mushroom spines. Harris et al. [11] have shown that thin and mushroom spines containing postsynaptic density markedly increase in the hippocampus between postnatal day 15 and adult ages, correlating with synaptic strength. Changes in spine numbers and morphology are associated with neuronal development and changes in neuronal activity. The spine shape is important for its function as the postsynaptic component of excitatory synapses [38]. Increases in spine formation and maturation are most likely related to increases in excitatory synapse formation. Application of exogenous Sema4D increased active RhoA in the whole cell lysate of cultured neurons. Furthermore, Sema4D-induced increase in spine density was almost completely blocked by treatment of ROCK inhibitor Y-27632 and also by introduction

Please cite this article in press as: X. Lin, et al., Sema4D-plexin-B1 implicated in regulation of dendritic spine density through RhoA/ROCK pathway, Neurosci. Lett. (2007), doi:10.1016/j.neulet.2007.09.045

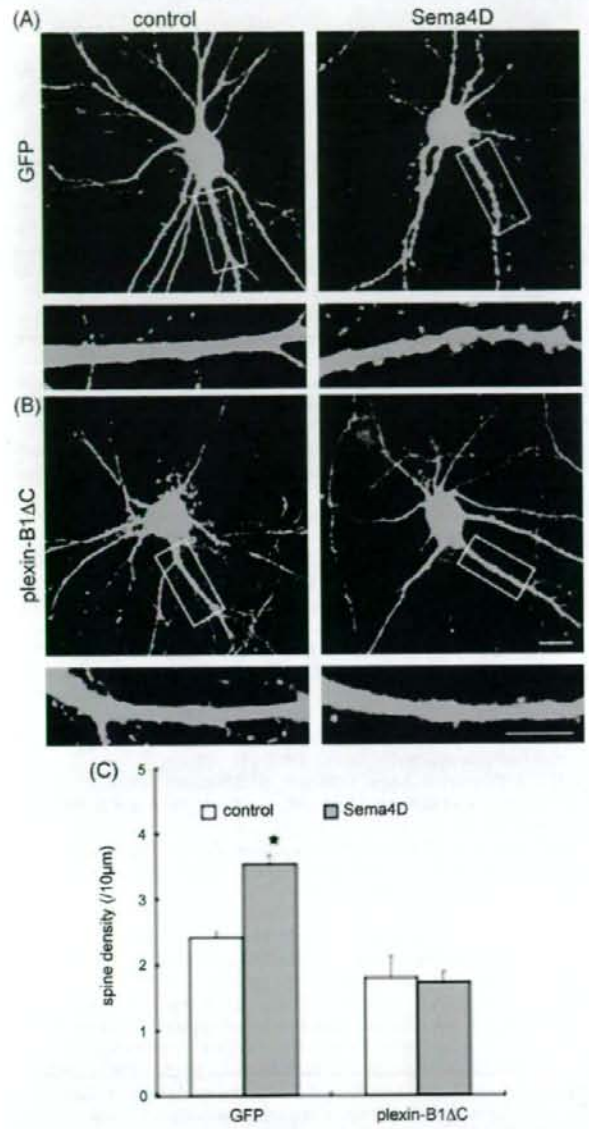


Fig. 4. C-terminus of plexin-B1 is required for the Sema4D effect on dendritic spines. (A and B) Confocal GFP-images were used to visualize dendritic morphology of cultured hippocampal neurons (21-DIV) transfected with GFP alone (A) and GFP with plexin-B1ΔC (B). Neurons were untreated (control) or treated with 1 nM Sema4D-Fc for 6 h. Scales: 10 μm (upper panels), 20 μm (lower panels). (C) Spine density (per 10 μm-segment) was quantified from 15 neurons as described above. $^{*}p < 0.001$ with Student *t*-text.

of plexin-B1ΔC mutant. These findings suggest that Sema4D-plexin-B1 regulate spine density and probably spine morphology through the association with PDZ-RhoGEFs and its downstream RhoA/ROCK pathway.

Rho GTPases play an important role in dendritic spine formation [38]. Overexpression of constitutively active RhoA in the hippocampal slices promotes spine elimination and reduced spine density, while dominant negative RhoA does not affect spine density [4,34] Whereas, either inhibition of RhoA using C3 exoenzyme or blockade of ROCK using Y-27632 reduces spine density and increases the length of spines [27,34]. In coincidence with these reports, ROCK inhibitor Y-27632 reduced spine density and increased the length of spines in this study. Either active form of RhoA or inhibitor of RhoA signaling reduces spine density, suggesting that the balance between active and inactive forms of RhoA is important in spine formation. Besides PDZ-RhoGEFs, Sema4D can induce activation of p190RhoGAP, a ubiquitous GAP in the brain, which leads to a decrease of active RhoA [3]. The negative RhoA regulator p190RhoGAP also plays an important role in the functional activities induced by Sema4D-plexin-B1 such as cell collapse, inhibition of integrin-based adhesion, and neurite outgrowth [3]. Thus, it is possible that the complex interactions among PDZ-RhoGEF, p190RhoGAP and plexin-B1 exquisitely control RhoA [3,21,23,33].

A recent study by Schubert et al. [31] have shown that high potassium-induced reduction of spine density is accompanied by a decrease of active RhoA in the synaptosomes but an increase in the whole cell lysates, suggesting that the local RhoA at the synapses is implicated in regulation of spine density. It remains to be examined how RhoA become active at the spines or is localized to the spines in a time-dependent manner after addition of Sema4D. Recently, by using RNAi knockdown, Paradis et al. [24] have shown that reduction of endogenous expression of Sema4D had no effect on glutamatergic synapses but decreased GABAergic synapse density. In this study, Sema4D at higher level than endogenous one resulted in an increase of spine density. Taken together, Sema4D might differently regulate the density of excitatory or inhibitory synapses in a concentration-dependent manner. It is intriguing to investigate whether excitatory glutamatergic synapses increase in number at higher Sema4D level after the addition of it.

## Acknowledgements

We are grateful to Dr. T. Nagase (Kazusa DNA Research Institute) for plasmids of KIAA0407 and KIAA0315, Dr. F. Suto (Nippon National Institute Genetics) for plexin-A1 and Dr. M. Uehata (Yoshitomi Pharmaceutical) for Y-27632. This study was supported in part by Grants-in aid for scientific research from the Ministry of Education, Science, Technology, Sports and Culture of Japan (SI).

## References

[1] K. Abe, O. Chisaka, F. Van Roy, M. Takeichi, Stability of dendritic spines and synaptic contacts is controlled by alpha N-catenin, Nat. Neurosci. 7 (2004) 357–363.
[2] G. Banker, K. Goslin, Culturing Nerve cell, MIT Press, London, 1993.
[3] D. Barberis, A. Casazza, R. Sordella, S. Corso, S. Artigiani, J. Settleman, P.M. Comoglio, L. Tamagnone, p190 Rho-GTPase activating protein associates with plexins and it is required for semaphorin signaling, J. Cell Sci. 11 (2005) 4689–4700.
[4] I.M. Ethell, E.B. Pasquale, Molecular mechanisms of dendritic spine development and remodeling, Prog. Neurobiol. 75 (2005) 161–205.

Please cite this article in press as: X. Lin, et al., Sema4D-plexin-B1 implicated in regulation of dendritic spine density through RhoA/ROCK pathway, Neurosci. Lett. (2007), doi:10.1016/j.neulet.2007.09.045

[5] I.M. Ethell, Y. Yamaguchi, Cell surface heparan sulfate proteoglycan syndecan-2 induces the maturation of dendritic spines in rat hippocampal neurons, J. Cell Biol. 144 (1999) 575–586.
[6] J.C. Fiala, M. Feinberg, V. Popov, K.M. Harris, Synaptogenesis via dendritic filopodia in developing hippocampal area CA1, J. Neurosci. 18 (1998) 8900–8911.
[7] M. Fischer, S. Kaech, D. Knutti, A. Matus, Rapid actin-based plasticity in dendritic spines, Neuron 20 (1998) 847–854.
[8] S. Fujioka, K. Masuda, M. Toguchi, Y. Ohoka, T. Sakai, T. Furuyama, S. Inagaki, Neurotrophic effect of semaphorin 4D in PC12 cells, Biochem. Biophys. Res. Commun. 301 (2003) 304–310.
[9] T. Furuyama, S. Inagaki, A. Kosugi, S. Noda, S. Saitoh, M. Ogata, Y. Iwahashi, N. Miyazaki, T. Hamaoka, M. Tohyama, Identification of a novel transmembrane semaphorin expressed on lymphocytes, J. Biol. Chem. 271 (1996) 33376–33381.
[10] R.J. Giger, R.J. Pasterkamp, S. Heijnen, A.J. Holtmaat, J. Verhaagen, Anatomical distribution of the chemorepellent semaphorin III/collapsin-1 in the adult rat and human brain: predominant expression in structures of the olfactory-hippocampal pathway and the motor system, J. Neurosci. Res. 52 (1998) 27–42.
[11] K.M. Harris, F.E. Jensen, B. Tsao, Three-dimensional structure of dendritic spines and synapses in rat hippocampus (CA1) at postnatal day 15 and adult ages: implications for the maturation of synaptic physiology and long-term potentiation, J. Neurosci. 12 (1992) 2685–2705.
[12] H. Hering, M. Sheng, Dendritic spines: structure, dynamics and regulation, Nat. Rev. Neurosci. 2 (2001) 880–888.
[13] M. Hirotani, Y. Ohoka, T. Yamamoto, H. Nirasawa, T. Furuyama, M. Kogo, T. Matsuya, S. Inagaki, Interaction of plexin-B1 with PDZ domain-containing Rho guanine nucleotide exchange factors, Biochem. Biophys. Res. Commun. 297 (2002) 32–37.
[14] S. Inagaki, Y. Ohoka, H. Sugimoto, S. Fujioka, M. Amasaki, H. Kurinami, N. Miyazaki, T. Furuyama, Sema4C, a transmembrane semaphorin, interacts with a post synaptic density protein, PSD-95, J. Biol. Chem. 276 (2001) 9174–9181.
[15] T. Kameyama, Y. Murakami, F. Suto, A. Kawakami, S. Takagi, T. Hirata, H. Fujisawa, Identification of plexin family molecules in mice, Biochem. Biophys. Res. Commun. 226 (1996) 396–402.
[16] A.L. Kolodkin, D.J. Matthes, C.S. Goodman, The semaphorin genes encode a family of transmembrane and secreted growth cone guidance molecules, Cell 75 (1993) 1389–1399.
[17] B.P. Liu, S.M. Strittmatter, Semaphorin-mediated axonal guidance via Rho-related G proteins, Curr. Opin. Cell Biol. 13 (2001) 619–626.
[18] Y. Luo, D. Raible, J.A. Raper, Collapsin, a protein in brain that induces the collapse and paralysis of neuronal growth cones, Cell 75 (1993) 217–227.
[19] K. Masuda, T. Furuyama, M. Takahara, S. Fujioka, H. Kurinami, S. Inagaki, Sema4D stimulates axonal outgrowth of embryonic DRG sensory neurons, Genes Cells 9 (2004) 821–829.
[20] N. Miyazaki, T. Furuyama, T. Sakai, S. Fujioka, Y. Ohoka, N. Takeda, S. Inagaki, Developmental localization of semaphorin H messenger RNA acting as a collapsing factor on sensory axons in the mouse brain, Neuroscience 93 (1999) 401–408.
[21] C. Moreau-Fauvarque, A. Kumanogoh, E. Camand, C. Jaillard, G. Barbin, I. Boquet, C. Love, E.Y. Jones, H. Kikutani, C. Lubetzki, I. Dusart, A. Chedotal, The transmembrane semaphorin Sema4D/CD100, an inhibitor of axonal growth, is expressed on oligodendrocytes and upregulated after CNS lesion, J. Neurosci. 23 (2003) 9229–9239.
[22] A.Y. Nakayama, M.B. Harms, L. Luo, Small GTPases Rac and Rho in the maintenance of dendritic spines and branches in hippocampal pyramidal neurons, J. Neurosci. 20 (2000) 5329–5338.
[23] I. Oinuma, H. Katoh, A. Harada, M. Negishi, Direct interaction of Rnd1 with Plexin-B1 regulates PDZ-RhoGEF-mediated Rho activation by Plexin-B1 and induces cell contraction in COS-7 cells, J. Biol. Chem. 278 (2003) 25671–25677.
[24] S. Paradis, D.B. Harrar, Y. Lin, A.C. Koon, J.L. Hauser, E.C. Griffith, L. Zhu, L.F. Brass, C. Chen, M.E. Greenberg, An RNAi-based approach identifies molecules required for glutamatergic and GABAergic synapse development, Neuron 53 (2007) 217–232.
[25] R.J. Pasterkamp, J.J. Peschon, M.K. Springgs, A.L. Kolodkin, Semaphorin7A promotes axon outgrowth through integrins and MAPKs, Nature 424 (2003) 398–405.
[26] V. Perrot, J. Vazquez-Prado, J.S. Gutkind, Plexin B regulates Rho through the guanine nucleotide exchange factors leukemia-associated Rho GEF (LARG) and PDZ-RhoGEF, J. Biol. Chem. 277 (2002) 43115–43120.
[27] Y. Pilpel, M. Segal, Activation of PKC induces rapid morphological plasticity in dendrites of hippocampal neurons via Rac and Rho-dependent mechanisms, Eur. J. Neurosci. 19 (2004) 3151–3164.
[28] F. Polleux, T. Morrow, A. Ghosh, Semaphorin 3A is a chemoattractant for cortical apical dendrites, Nature 404 (2000) 567–573.
[29] X.D. Ren, M.A. Schwartz, Determination of GTP loading on Rho, Methods Enzymol. 325 (2000) 264–272, C.
[30] C. Sala, K. Futai, K. Yamamoto, P.F. Worley, Y. Hayashi, M. Sheng, Inhibition of dendritic spine morphogenesis and synaptic transmission by activity-inducible protein Homer1a, J. Neurosci. 23 (2003) 6327–6337.
[31] V. Schubert, J.S. Da Silva, C.G. Dotti, Localized recruitment and activation of RhoA underlies dendritic spine morphology in a glutamate receptor-dependent manner, J. Cell Biol. 172 (2006) 453–467.
[32] Semaphorin Nomenclature Committee, Unified nomenclature for the semaphorins/collapsins, Cell 97 (1999) 551–552.
[33] J.M. Swiercz, R. Kuner, J. Behrens, S. Offermanns, Plexin-B1 directly interacts with PDZ-RhoGEF/LARG to regulate RhoA and growth cone morphology, Neuron 35 (2002) 51–63.
[34] A. Tashiro, A. Minden, R. Yuste, Regulation of dendritic spine morphology by the rho family of small GTPases: antagonistic roles of Rac and Rho, Cereb. Cortex 10 (2000) 927–938.
[35] M. Uehata, T. Ishizaki, H. Satoh, T. Ono, T. Kawahara, T. Morishita, H. Tamakawa, K. Yamagami, J. Inui, M. Maekawa, S. Narumiya, 7 Calcium sensitization of smooth muscle mediated by a Rho-associated protein kinase hypertension, Nature 389 (1997) 990–994.
[36] T. Worzfeld, A.W. Puschel, S. Offermanns, R. Kuner, Plexin-B family members demonstrate non-redundant expression patterns in the developing mouse nervous system: an anatomical basis for morphogenetic effects of Sema4D during development, Eur. J. Neurosci. 19 (2004) 2622–2632.
[37] T. Yamada, Y. Ohoka, M. Kogo, S. Inagaki, Physical and functional interactions of the lysophosphatidic acid receptors with PDZ domain-containing Rho guanine nucleotide exchange factors (RhoGEFs), J. Biol. Chem. 280 (2005) 19358–19363.
[38] R. Yuste, T. Bonhoeffer, Morphological changes in dendritic spines associated with long-term synaptic plasticity, Ann. Rev. Neurosci. 24 (2001) 1071–1089.

Please cite this article in press as: X. Lin, et al., Sema4D-plexin-B1 implicated in regulation of dendritic spine density through RhoA/ROCK pathway, Neurosci. Lett. (2007), doi:10.1016/j.neulet.2007.09.045

Cell PRESS

Neuron
Article

# Activity-Induced Protocadherin Arcadlin Regulates Dendritic Spine Number by Triggering N-Cadherin Endocytosis via TAO2β and p38 MAP Kinases

Shin Yasuda,[1,6] Hidekazu Tanaka,[2,6,*] Hiroko Sugiura,[1,6] Ko Okamura,[2] Taiki Sakaguchi,[2] Uyen Tran,[4] Takako Takemiya,[1] Akira Mizoguchi,[3] Yoshiki Yagita,[5] Takeshi Sakurai,[5] E.M. De Robertis,[4] and Kanato Yamagata[1,*]

[1]Department of Neuropharmacology, Tokyo Metropolitan Institute for Neuroscience, Fuchu, Tokyo 183-8526, Japan
[2]Department of Pharmacology, Osaka University Medical School, Suita, Osaka 565-0871, Japan
[3]Department of Anatomy, Mie University School of Medicine, Tsu, Mie 514-8507, Japan
[4]Howard Hughes Medical Institute and Department of Biological Chemistry, University of California, Los Angeles, Los Angeles, CA 90095-1662, USA
[5]Department of Neuroscience, Mount Sinai School of Medicine, New York, NY 10128, USA
[6]These authors contributed equally to this work.
*Correspondence: htanaka@pharma1.med.osaka-u.ac.jp (H.T.), kyamagat@tmin.ac.jp (K.Y.)
DOI 10.1016/j.neuron.2007.08.020

## SUMMARY

**Synaptic activity induces changes in the number of dendritic spines. Here, we report a pathway of regulated endocytosis triggered by arcadlin, a protocadherin induced by electroconvulsive and other excitatory stimuli in hippocampal neurons. The homophilic binding of extracellular arcadlin domains activates TAO2β, a splice variant of the thousand and one amino acid protein kinase 2, cloned here by virtue of its binding to the arcadlin intracellular domain. TAO2β is a MAPKKK that activates the MEK3 MAPKK, which phosphorylates the p38 MAPK. Activation of p38 feeds-back on TAO2β, phosphorylating a key serine required for triggering endocytosis of N-cadherin at the synapse. Arcadlin knockout increases the number of dendritic spines, and the phenotype is rescued by siRNA knockdown of N-cadherin. This pathway of regulated endocytosis of N-cadherin via protocadherin/TAO2β/MEK3/p38 provides a molecular mechanism for transducing neuronal activity into changes in synaptic morphologies.**

## INTRODUCTION

Various cellular events have been correlated with synaptic plasticity, a mechanism that is believed to underlie learning and memory. Cell-adhesion molecules are among the proteins responsible for these cellular events (Bailey et al., 1992; Manabe et al., 2000; Sytnyk et al., 2006). Among them, N-cadherin, a classical cadherin cell-adhesion molecule abundantly expressed in hippocampal excitatory synaptic junctions, has been most intensely correlated with synaptic plasticity (Bozdagi et al., 2000; Murase et al., 2002; Okamura et al., 2004; Tanaka et al., 2000; Tang et al., 1998). In a previous study, we found that an activity-regulated synaptic cell-adhesion molecule, arcadlin, is also essential for synaptic plasticity (Yamagata et al., 1999). Arcadlin, the rat ortholog of human protocadherin-8 (pcdh8) and of mouse, *Xenopus*, and zebrafish paraxial protocadherin (PAPC), is a unique member of the protocadherin superfamily and has a distinct cytoplasmic region (Strehl et al., 1998; Yamagata et al., 1999; Yamamoto et al., 2000). In *Xenopus* and zebrafish, arcadlin/PAPC plays an important role in homophilic cell adhesion and gastrulation movements of the paraxial mesoderm (Kim et al., 1998; Yamamoto et al., 2000). Recently, *Xenopus* arcadlin/PAPC has been shown to downregulate the adhesion activity of C-cadherin, a classical cadherin of developing *Xenopus* (Chen and Gumbiner, 2006). The interacting partners of arcadlin/PAPC in the CNS have not been identified.

The activity of cell-adhesion molecules in synaptic membranes is regulated in part by endocytosis. ApCAM, an *Aplysia* neural cell-adhesion molecule, for example, becomes internalized in presynaptic membrane upon the acquisition of long-term potentiation (LTP) (Bailey et al., 1992). Clathrin-coated pits and vesicles have been found in postsynaptic dendritic spines (Cooney et al., 2002; Racz et al., 2004). One of the mechanisms that regulate the endocytosis involves p38 MAPK (Johnson and Lapadat, 2002; Zhu et al., 2002), a serine/threonine kinase that responds to various stress-related stimuli (Tibbles and Woodgett, 1999). TAO2, a MAP kinase kinase kinase (MAPKKK) initially isolated as a mammalian homolog of Ste20p in *S. cerevisiae* (Chen et al., 1999), serves as a regulator of the p38 MAPK. Extracellular stimuli, such as those of certain G protein-coupled receptors or insulin receptor, are transduced via TAO kinases to p38 MAPK in nonneural tissues (Chen et al., 2003). The p38 MAPK is highly expressed in the brain, where it is thought to be involved in synaptic plasticity (Thomas and Huganir, 2004). The functions of TAO kinases and their upstream receptors in the CNS are not known.

In this study, we have found that N-cadherin, the most abundant classical cadherin in hippocampal excitatory synapses (Benson and Tanaka, 1998), serves as a target of arcadlin/PAPC in the mammalian nervous system. Arcadlin is induced by neural stimulation and transported to the synaptic membrane, where it binds to and internalizes N-cadherin. During our investigations into the mechanism of this internalization, we cloned a spliced form of TAO2 kinase (TAO2β) that binds to the arcadlin intracellular domain. Homophilic interactions of arcadlin on the cell surface activate p38 MAPK through the activation of TAO2β. In turn, active p38 MAPK feeds-back on TAO2β, phosphorylating its carboxy-terminal domain at a specific serine. This triggers the coendocytosis of an N-cadherin-arcadlin complex. Furthermore, knockout of *arcadlin* in the mouse leads to an increase in dendritic spines in cultured neurons, and siRNA knockdown of N-cadherin recovered the spine density. We propose that endocytosis regulated by this signal transduction pathway involving a protocadherin, a MAPKKK that binds to its intracellular domain, a MAPK, and a classical cadherin regulates the adhesiveness of synaptic membranes and hence the number of spines in an activity-dependent way.

## RESULTS

### Arcadlin Interacts with N-Cadherin

Arcadlin is an activity-regulated cell-adhesion molecule whose expression level is very low in the resting brain but is vigorously induced by neural stimulation and recruited to the dendritic spine (Yamagata et al., 1999). Upon neural stimulation, such as maximal electroconvulsive seizure (MECS), arcadlin immunoreactivity increased and displayed a punctate distribution in the stratum lucidum of the hippocampal CA3 region, in which N-cadherin is also found (Figures 1A and 1B; Fannon and Colman, 1996).

In cultured hippocampal neurons, spontaneous synaptic activity causes detectable expression of arcadlin, which was increased by brief treatment with glutamate or elevation in cAMP with isobutyl methylxanthine (IBMX) and forskolin (Figures 1C and 1D and data not shown). Although N-cadherin is also known to be induced by elevating cAMP level in acute hippocampal slices (Bozdagi et al., 2000), there was no significant induction of N-cadherin in our culture (Figures 1C and 1D). This discrepancy is presumably due to the lack of glial support and the higher spontaneous activity of neurons in dispersed culture. The expression of arcadlin in cultures treated with IBMX and forskolin was confined to glutamate decarboxylase 65 (GAD6)-negative, non-GABAergic neurons (Figure 1E, arrow). In such neurons, arcadlin showed punctate distribution in dendrites (Figure 1F, arrow). The arcadlin puncta were not colocalized or apposed to the GAD6-puncta, which correspond to inhibitory axonal termini (Figure 1F, arrowhead). In contrast, the arcadlin-puncta colocalized with postsynaptic markers for excitatory synapses, such as PSD-95 and the NMDA receptor subunit NR1, as well as N-cadherin (Figure 1G). Arcadlin was expressed in developing axonal growth cones of young neurons, showing that arcadlin is also present in developing presynaptic membranes (Figure 1H, arrow).

We discovered the association of arcadlin with N-cadherin fortuitously during the course of immunoprecipitation studies of N-cadherin in hippocampal lysates. Arcadlin was coimmunoprecipitated with N-cadherin in dissected rat hippocampi 4 hr after electroconvulsions, but very little was found in unstimulated hippocampi (Figure 1I; note that the amount of β-catenin bound to N-cadherin is not affected). Coimmunoprecipitation was detectable in resting cultured neurons, which was increased by neural stimulation, such as depolarization by KCl (Figure 1J). Another synaptic classical cadherin, cadherin-11, was also found to be associated with the induced arcadlin in the brain (Figure 1K). The fact that arcadlin is targeted to multiple classical cadherins is reminiscent of the notion that *Xenopus* arcadlin/PAPC downregulates the adhesion activity of C-cadherin (Chen and Gumbiner, 2006). In this study, we focused on N-cadherin as the most abundant example of these cadherins. Coimmnoprecipitation experiments from cocultured cell lines transfected with *N-cadherin* and *arcadlin* independently (single transfections) or simultaneously (cotransfection) revealed that they associated laterally in the same membrane (Figure 1L). Consistently, we were able to localize their interaction domains to their transmembrane segments by deletion mutant analyses (Figures 1M and 1N). The affinity of N-cadherin to arcadlin was significantly reduced by a point mutation L561P or L561P/M562G in the middle of the transmembrane α-helix of N-cadherin (Figures 1M and 1O). The corresponding amino acid of E-cadherin plays a pivotal role in homophilic *cis* dimerization (Huber et al., 1999).

### Arcadlin Induces the Internalization of N-Cadherin

To test whether arcadlin had any effect on the adhesive activity of N-cadherin, we performed cell-aggregation assays using L929 cells (Takeichi, 1977). Although arcadlin itself has a homophilic adhesive activity, it is too weak to be detected in the aggregation assay optimized for classical cadherins (Yamagata et al., 1999). We found that arcadlin downregulated the homophilic adhesiveness of N-cadherin (Figures 2A and 2B). The inhibitory effect was not attributable to either the expression level of N-cadherin (Figure 2C) or the intracellular molecules associated with N-cadherin, such as catenins (Figure 2D). We therefore hypothesized that the downregulation of N-cadherin activity could involve the internalization of N-cadherin by analogy to the case of apCAM (Bailey et al., 1992) and L1 (Kamiguchi and Lemmon, 2000). Recently, a key role for endocytosis in the disassembly of E-cadherin cell-cell adhesion has been reported (Troyanovsky et al., 2006).

To examine whether arcadlin enhances the internalization of N-cadherin, we first quantified surface N-cadherin level by labeling neuronal proteins on the extracellular surface with biotin. The biotin-labeled surface proteins were

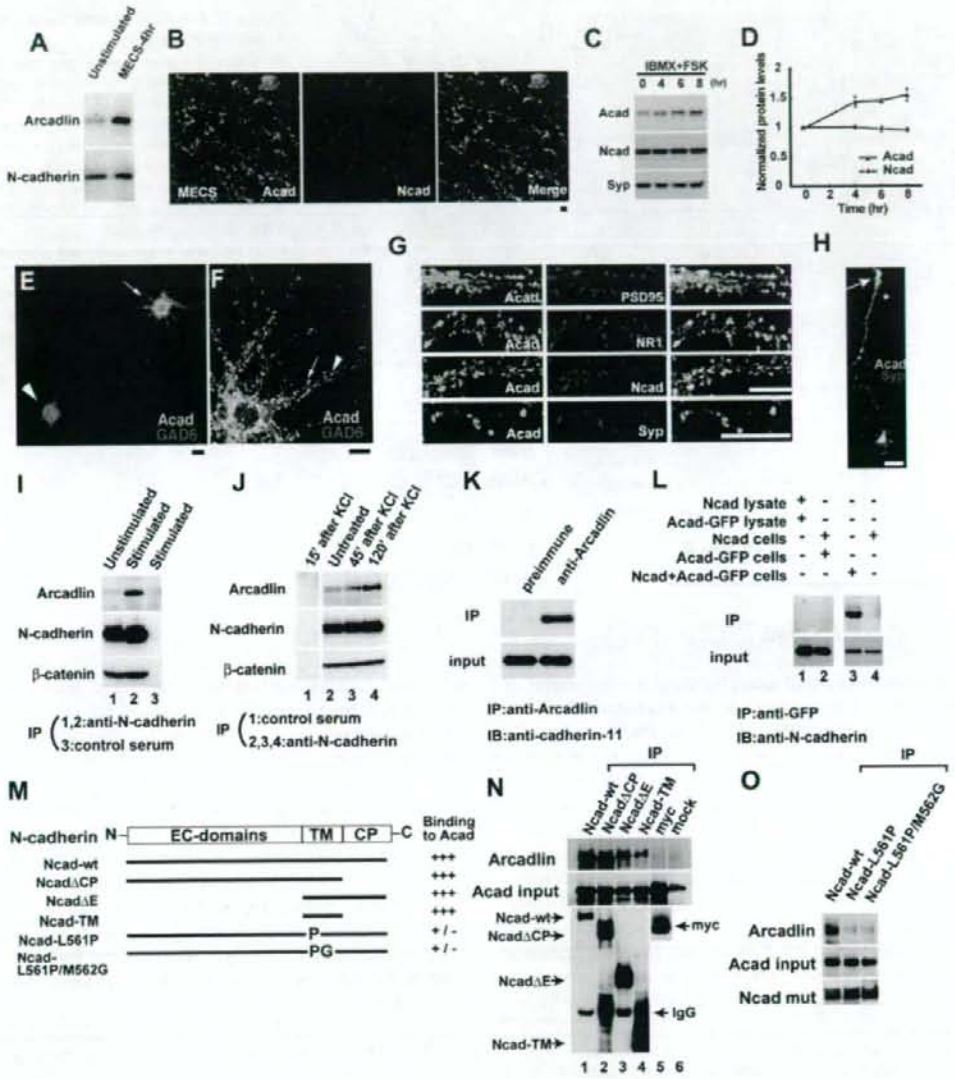


**Figure 1. Arcadlin Is Associated with N-Cadherin at Hippocampal Synaptic Puncta**

(A) Hippocampal extracts from unstimulated (control) and electroconvulsive shocked (MECS-4hr) rats were immunoblotted for arcadlin and N-cadherin.

(B) CA3 stratum lucidum doubly immunolabeled for arcadlin (Acad, green) and N-cadherin (Ncad, red) 4 hr after MECS. Significant colocalization confirmed ($r = 0.51$).

(C) Elevation of cAMP by IBMX and forskolin (FSK) induces the expression of arcadlin in cultured hippocampal neurons as examined by immunoblots. Syp, synaptophysin.

(D) The graph shows the relative band intensities of arcadlin and N-cadherin normalized with the bands for synaptophysin (mean ± SEM).

(E) Hippocampal neurons treated with IBMX and forskolin for 4 hr and immunostained for arcadlin (green) and GAD6 (red).

(F) An excitatory neuron double labeled for arcadlin (green) and GAD6 (red).

(G) Neurons double labeled for arcadlin (green) and PSD-95 (red; $r = 0.43$), NR1 (red), N-cadherin (red; $r = 0.36$), or synaptophysin (red).

(H) Hippocampal neuron (3 DIV) stained for arcadlin (green) and synaptophysin (red).

(I) Immunoprecipitation of N-cadherin from unstimulated (lane 1) and MECS-treated (lane 2) rat hippocampal extracts, immunoblotted for arcadlin (top), N-cadherin (middle), and β-catenin (bottom). Lane 3, control preimmune serum.

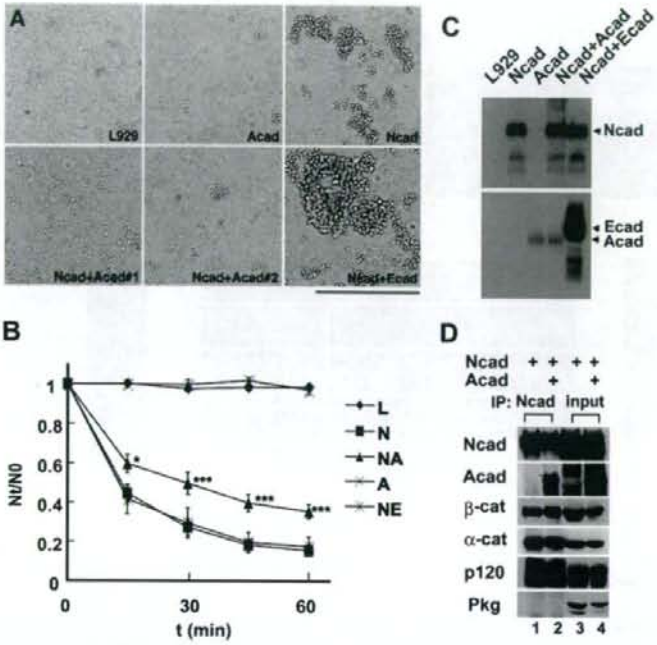


**Figure 2. Arcadlin Inhibits the Adhesive Activity of N-Cadherin**

(A) Cell-aggregation assay was performed using L929 cells stably transfected with *N-cadherin* (Ncad), *arcadlin* (Acad), and both (Ncad + Acad #1 and Ncad + Acad #2; two independent transfected cell lines). Scale bar, 500 μm.

(B) Adhesive activity was quantified by counting the number of aggregates (mean ± SEM) at indicated times (Nt). $^{*}p < 0.05$, $^{***}p < 0.001$, compared to Ncad.

(C) N-cadherin expression level of each cell type was examined by western blot.

(D) COS7 cells were doubly transfected with *N-cadherin* and *arcadlin* (lanes 2 and 4) or *N-cadherin* and *mock* (lanes 1 and 3), immunoprecipitated with the antibody against N-cadherin, and subjected to immunoblot (lanes 1–2). Lanes 3–4, inputs.

isolated with avidin-sepharose beads and immunoblotted for N-cadherin (Figure 3A). Membrane depolarization with KCl and elevating cAMP level, both of which induced endogenous arcadlin (Figures 1C, 1D, and 1J), resulted in significant reduction in surface N-cadherin levels (Figures 3A and 3B), whereas surface levels of neuroligin, as a control, did not change (Figures 3C and 3D).

Next, we quantified the amount of surface-associated N-cadherin microscopically. We generated a new polyclonal antibody, MT79, which recognizes the extracellular domain of N-cadherin (see Figure S1 in the Supplemental Data available with this article online). Mouse hippocampal neurons at age 14–17 days were incubated in medium containing anti-N-cadherin MT79 antibody at 4°C for 30 min. Surface-associated N-cadherins were then labeled with the secondary antibody without permeabilization of plasma membrane (Figure 3E, green). To analyze the synaptic population, we examined the N-cadherin signal that overlapped with synaptophysin (Figure 3G; synaptic versus extrasynaptic). A 33.4% ± 5.1% decrease in the mean intensity of total surface N-cadherin in the IBMX + forskolin treatment group relative to control was observed (Figures 3F and 3G). (The mean intensity of synaptophysin did not differ between groups.) The decrease in the surface N-cadherin mean intensity was observed in both the synaptic (synaptophysin-overlapping fraction) and extrasynaptic (synaptophysin-nonoverlapping fraction) populations.

(J) Immunoprecipitation of N-cadherin from cultured neurons stimulated with 25 mM KCl for 1 min and further cultured for 45–120 min, immunoblotted for arcadlin (top), N-cadherin (middle), and β-catenin (bottom). Lane 1, control preimmune serum.

(K) Immunoprecipitation of arcadlin from MECS-treated rat brain extracts, immunoblotted for cadherin-11. Left, control preimmune serum.

(L) COS7 cells were transfected with *arcadlin-EGFP* and/or *N-cadherin* and subjected to immunoprecipitation with anti-GFP serum followed by immunoblot with anti-N-cadherin antibody (top). Bottom, input. Lane 1, the lysate of *N-cadherin*-transfected cells was mixed in vitro with the lysate of *arcadlin*-transfected cells. Lane 2, arcadlin-expressing cells and N-cadherin-expressing cells were cocultured. Lane 3, *arcadlin* and *N-cadherin* were cotransfected. Lane 4, a control without transfecting *arcadlin-EGFP*. The lack of coimmunoprecipitation in lanes 1 and 2 suggested that these molecules do not interact in vitro or in *trans*, but associate laterally in the same membrane.

(M) N-cadherin mutants including wild-type (*Ncad-wt*), cytoplasmic domain deleted (*NcadΔCP*), extracellular domain deleted (*NcadΔE*), transmembrane segment alone (*Ncad-TM*), and point mutated in the middle of transmembrane region (*Ncad-L561P*, *Ncad-L561P/M562G*) were examined for the binding to full-length *arcadlin*. *N-cadherin* mutants fused with *myc*-tag were cotransfected with *arcadlin* into COS7 cells and immunoprecipitated with anti-myc antibody.

(N) Top, blot of arcadlin coimmunoprecipitated with the indicated N-cadherin mutants (lanes 1–4) or controls (lanes 5 and 6). In lane 2, abundant NcadΔCP (invisible) pushes the arcadlin band down to the lower molecular size position. Middle, arcadlin input. Bottom, immunoprecipitated N-cadherin mutants (myc probed).

(O) Top, blot of arcadlin coimmunoprecipitated with the indicated N-cadherin point mutants. Middle, arcadlin input. Bottom, immunoprecipitated N-cadherin mutants (myc probed).

Scale bars, 10 μm.

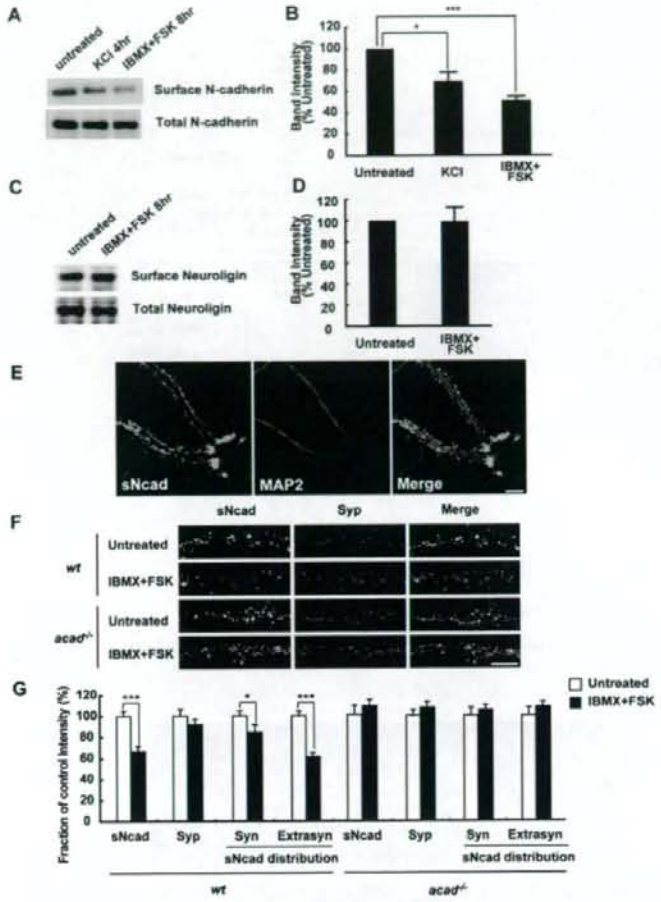


**Figure 3. Depolarization or Elevated cAMP Level Increases N-Cadherin Internalization through an Arcadlin-Dependent Pathway**

(A) Neuronal cell surface protein biotinylated and isolated with avidin-sepharose was immunoblotted for N-cadherin. Bottom, total protein.

(B) Densitometric quantification of surface N-cadherin levels. Surface protein levels were normalized with total protein levels and shown as proportion to the control experiment (%, mean ± SEM). n = 6.

(C) Neuronal cell surface protein was immunoblotted for neuroligin. Bottom, total protein.

(D) Densitometric quantification of surface neuroligin levels. Surface protein levels were normalized with total protein levels and shown as proportion to the control experiment (%, mean ± SEM). n = 5.

(E) Live neurons were incubated with anti-N-cadherin extracellular domain antibody (MT79) at 4°C for 30 min. Surface N-cadherin (sNcad) was labeled with Alexa-488-conjugated secondary antibody without membrane permeabilization (green). MAP2 was subsequently labeled after the permeabilization (red).

(F) Pretreatment of the neurons with IBMX and forskolin resulted in a decrease in surface N-cadherin intensity (green). Red, synaptophysin (Syp). Note that the change in surface N-cadherin intensity is not obvious in *acad/papc*$^{-/-}$ neurons.

(G) Quantification of surface N-cadherin intensity (mean ± SEM). The change in the surface N-cadherin mean intensity was observed in both the synaptophysin-overlapping fraction (Syn) and synaptophysin-nonoverlapping fraction (Extrasyn) populations. n = 40–50 dendrites from 4–5 independent experiments.

*p < 0.05, ***p < 0.001. Scale bars, 10 μm.

To show that the cAMP (IBMX + forskolin)-induced internalization of N-cadherin was indeed mediated by arcadlin, we utilized *arcadlin (acad/papc)*$^{-/-}$ mice (Yamamoto et al., 2000). The *acad*$^{-/-}$ mice were apparently normal, and the gross expression level of N-cadherin appeared the same as wild-type in brain sections and cultured neurons (data not shown). Neurons cultured from *acad*$^{-/-}$ mice extended dendrites and axons normally. The surface N-cadherin intensity of *acad*$^{-/-}$ neurons was slightly higher than that of *acad*$^{+/+}$ neurons (9.8% ± 3.6% increase in biotinylation assay, n = 5) and of *acad*$^{+/-}$ neurons (37.9 ± 1.3 [n = 100] versus 33.1 ± 0.9 [n = 100], arbitrary fluorescence units in microscopic analysis, data collected from ten independent experiments). In these *acad*$^{-/-}$ neurons, there was no significant change in the mean intensity of total surface N-cadherin in the IBMX + forskolin treatment group relative to control (Figures 3F and 3G). The data indicate that the IBMX + forskolin treatment-induced N-cadherin internalization is mediated by arcadlin.

### Identification of an Isoform of TAO2 Kinase as a Signal Transducer of Arcadlin

To dissect the molecular mechanism of endocytosis of N-cadherin by arcadlin, we searched for an intracellular binding partner of arcadlin. A splice form of TAO2 kinase was cloned in a yeast two-hybrid screen using a cDNA library prepared from electroconvulsed rat hippocampi and the cytoplasmic domain of arcadlin as bait (Figure 4A and Figure S2). This isoform of TAO2 kinase (named TAO2β) of 1056 amino acids shares the common serine/threonine protein kinase catalytic domain and the MEK binding domain with the original TAO2 kinase (renamed as TAO2α hereafter) but has a unique carboxy-terminal regulatory domain that shows no apparent homology to any known protein motif (Figure 4A and Figure S2B). The mRNA portion corresponding to the C-terminal domain of TAO2α is transcribed from only one exon, whereas that encoding the TAO2β C terminus is derived partly from the same exon, and mostly from three downstream exons,

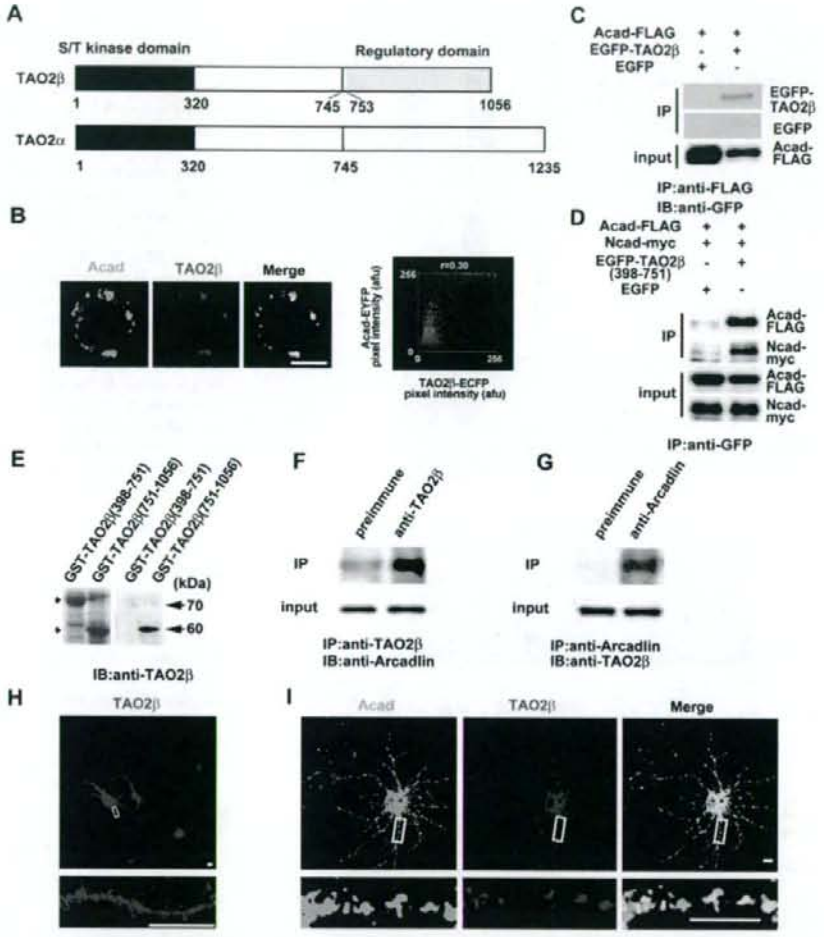


**Figure 4. TAO2β Binds to the Intracellular Domain of Arcadlin**

(A) Diagram of TAO2 kinases. An isoform of TAO2 (TAO2β) was identified as an intracellular binding partner of arcadlin. The original TAO2 was renamed as TAO2α. Most of the C-terminal regulatory domain of TAO2β (aa 753–1056) is distinct from that of TAO2α.

(B) Typical fluorescence image (left) and scatterplot (right) of HEK293T cells coexpressing TAO2β-ECFP and arcadlin-EYFP. Significant colocalization confirmed ($r = 0.30$).

(C) Arcadlin-FLAG was immunoprecipitated (IP) from HEK293T cells transfected with *arcadlin-flag* and *EGFP-tao2β* and immunoblotted (IB) with anti-GFP serum.

(D) EGFP-TAO2β(398-751) or control EGFP was immunoprecipitated with anti-GFP serum (IP) from HEK293T cells transfected with *arcadlin-flag*, *N-cadherin-myc*, and *EGFP-tao2β(398–751)* and immunoblotted for arcadlin (anti-FLAG) and N-cadherin (anti-myc). Left, transfected with *EGFP* instead of *EGFP-tao2β(398–751)*.

(E) The affinity purified anti-TAO2β antibody recognized the unique regulatory domain specific for the β isoform. Left, CBB protein staining.

(F) Hippocampal extract immunoprecipitated with anti-TAO2β antibody and immunoblotted for arcadlin.

(G) Hippocampal extract immunoprecipitated with anti-arcadlin antibody and immunoblotted for TAO2β.

(H) Cultured neurons were immunostained for TAO2β.

(I) Confocal live imaging of arcadlin-EYFP (green) and TAO2β-ECFP (red) expressed in dendrites.

Scale bars, 10 μm.

suggesting that *tao2α* and *-β* mRNAs are alternative splicing products from the same gene (Figure S2A).

A recombinant TAO2β tagged at its carboxyl terminus with enhanced cyan fluorescent protein (TAO2β-ECFP) colocalized with arcadlin-EYFP (enhanced yellow fluorescent protein) in HEK293T cells (Figure 4B). The molecular interaction between these proteins was confirmed by coimmunoprecipitation (Figure 4C). The formation of a

trimeric complex of TAO2β, arcadlin, and N-cadherin was confirmed in triple-transfected HEK293T cells (Figure 4D). The association of EGFP-TAO2β (398–751), the central domain common to both α and β isoforms, suggested that TAO2α can also bind to arcadlin (Figure 4D). In order to examine in vivo interactions of TAO2β, we produced and purified a polyclonal antibody recognizing the carboxy-terminal domain specific for the β isoform of TAO2 kinase (Figure 4E). Coimmunoprecipitation of endogenous arcadlin protein with the anti-TAO2β antibody (Figure 4F) and, reciprocally, of TAO2β with anti-arcadlin antibody (Figure 4G) confirmed that these molecules associate in vivo in MECS-treated rat hippocampi. Immunolocalization of TAO2β showed puncta in dendrites (Figure 4H). Arcadlin-EYFP and TAO2β-ECFP transfected into cultured hippocampal neurons colocalized in dendrites (Figure 4I). We conclude that the arcadlin protocadherin and the TAO2β MAPKKK interact in hippocampal neurons.

### Arcadlin Homophilic Interaction Triggers Activation of p38 MAPK and Internalization

The arcadlin/PAPC extracellular domain mediates homophilic binding (Chen and Gumbiner, 2006; Kim et al., 1998; Yamagata et al., 1999). In addition, arcadlin is a transiently expressed protein in hippocampal neurons, whose protein level peaks at 4 hr after the synaptic stimulation and largely disappears within 8 hr (Yamagata et al., 1999). During this period, the arcadlin protein is transported to pre- and postsynaptic membranes and rapidly turned over (Yamagata et al., 1999). In HEK293T cells cotransfected with *arcadlin-EGFP* and *arcadlin-flag*, arcadlin-arcadlin lateral interactions in the same membrane were readily detectable (Figure 5A, lane3). To analyze *trans* interactions specifically, we utilized arcadlin-L, a splice variant of arcadlin containing a 98 amino acid insertion in its cytoplasmic region. Arcadlin-L-EGFP-expressing cells and arcadlin-L-FLAG-expressing cells were cocultured so that these two types of cells attached to each other. Immunoprecipitation of arcadlin-L-EGFP with anti-flag antibody indicated that there is significant binding activity in *trans* (Figure 5A, lane 1). Application of a soluble extracellular fragment of recombinant arcadlin protein (Acad-EC, purified via a His-tag) into the culture medium competed *trans*-association, indicating that Acad-EC binds to the extracellular domain of arcadlin in *trans* (Figure 5A, lane 2). Although *cis* interaction may be also involved, Acad-EC at this concentration was not sufficient to replace the lateral oligomerization (data not shown).

Arcadlin molecules expressed in HEK293T cells abundantly localized to the cell surface. There was also detectable fraction of arcadlin in intracellular vesicles (Figure 5B, 0 min). Homophilic interaction of arcadlin on the cell surface with Acad-EC added to the culture medium triggered the rapid translocation of arcadlin from the periphery to the center of HEK293T cells cotransfected as described below (Figure 5B). This shift is mediated by endocytosis, because the moved arcadlin colocalized with EGFP-rab5 as a marker for endosomes and because the internalization of arcadlin was blocked by a coexpression of a dominant-negative form of dynamin, as shown in Figures 5B and 5G. A similar endocytic response was observed upon the application of the antibody against the extracellular region of arcadlin (data not shown). Therefore, a binding of the extracellular domain is sufficient to enhance the endocytosis of arcadlin. We next used this Acad-EC reagent to investigate the signal transduction mechanism that triggers endocytosis. It should be noted that a detectable level of background arcadlin endocytosis before the addition of Acad-EC may be triggered by the *cis* homophilic interaction of the transfected arcadlin (Figure 5B, 0 min).

Because TAO2β forms a molecular complex with the arcadlin intracellular domain, we asked whether p38 MAPK, a main target kinase of the TAO2α-MAPKKK pathway bridged by MEK3 (MAPKK-3) (Chen et al., 2003), was activated by the arcadlin signal. HEK293T cells cotransfected with *arcadlin*, *tao2β*, *MEK3*, and *p38 MAPK* were treated by addition of purified Acad-EC (10 μg/ml) to the culture medium. Immunostaining and immunoblot of the phosphorylated forms of p38 MAPK and MEK3 revealed that the phosphorylation levels of both kinases were enhanced within 30 min of the application of Acad-EC (Figures 5B and 5C). The p38 MAPK phosphorylation is mediated by arcadlin and TAO2β, because Acad-EC did not exert any response in HEK293T cells lacking either *arcadlin* or *tao2β* transfection (Figure 5D). Importantly, addition of Acad-EC protein triggered the activation of endogenous p38 MAPK in the dendritic shaft of primary cultures of rat hippocampal neurons (Figure 5E). Taken together, the results suggest that the arcadlin extracellular domain activates p38 MAPK via TAO2β. In cultured neurons, activation of p38 was detected specifically in the dendritic shaft after addition of protocadherin extracellular domain.

### TAO2β Is Required for p38 Activation and Endocytosis of Arcadlin

We then addressed whether TAO2β is necessary for the phosphorylation of p38 MAPK and the endocytosis of arcadlin. We reconstituted the arcadlin-TAO2β-MEK3-p38 MAPK signaling pathway in HEK293T cells by cotransfecting *arcadlin* with *tao2β*, *tao2βK57A* (catalytically defective TAO2 kinase; Chen et al., 2003), or *tao2α*. After the treatment with Acad-EC for 30 min, cells were analyzed for the phosphorylation of p38 MAPK (Figure 5F) and endocytosis of arcadlin by the surface biotinylation assay (Figure 5G). The phosphorylation of p38 MAPK was significantly increased, and surface arcadlin levels were significantly reduced in cells expressing wild-type TAO2β (Figures 5F and 5G). In *mock* or *tao2βK57A*-transfected cells, neither the endocytosis of arcadlin nor the phosphorylation of p38 MAPK was observed (Figures 5F and 5G). Cells expressing TAO2α displayed full activation of p38 MAPK but were deficient in the internalization of arcadlin (Figures 5F and 5G). We conclude from these data that the kinase

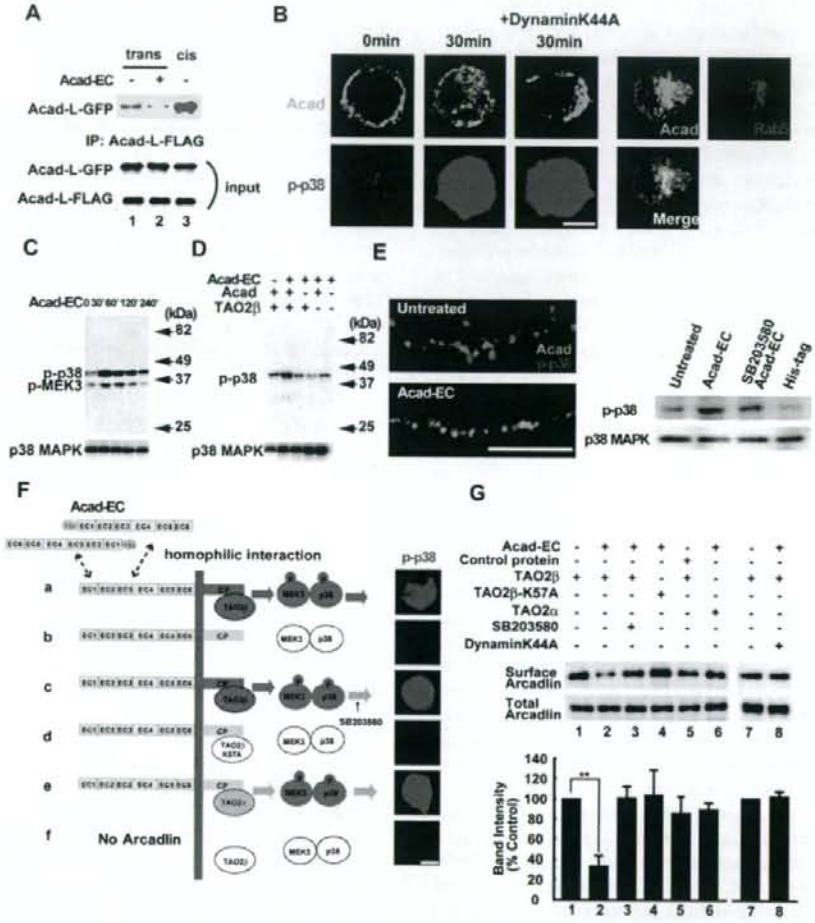


**Figure 5. Homophilic Interaction of Arcadlin Causes Internalization via the Activation of Arcadlin-TAO2β-p38 MAPK Signaling Pathway**

(A) Arcadlin-L-GFP or arcadlin-L-FLAG were expressed on different cell surfaces independently and allowed to interact across the cell-cell junction in mixed cell culture and were immunoprecipitated with anti-FLAG antibody followed by immunoblot for GFP (top). Bottom, input. Acad-EC protein added in the culture medium inhibited the *trans*-interaction (lane 2, compared with lane 1). Lane 3, cotransfection of *arcadlin-I-EGFP* and *arcadlin-I-flag*, which allows *cis*-interaction.

(B) HEK293T cells transfected with *arcadlin*, *tao2β*, *MEK3*, and *p38 MAPK* were treated with Acad-EC (10 μg/ml, 30 min) and immunostained. *dynaminK44A* (center) or *EGFP-rab5* (right) was additionally cotransfected. Surface and cytoplasmic localizations were revealed by optical sectionings by a confocal microscope.

(C) Extracts of HEK293T cells transfected with *arcadlin*, *tao2β*, *MEK3*, and *p38 MAPK* and treated with Acad-EC were immunoblotted for phospho-p38 MAPK and phospho-MEK3.

(D) Extracts of HEK293T cells with or without transfection of *arcadlin* and *tao2β* were immunoblotted for p38 phosphorylation upon the addition of Acad-EC to culture medium.

(E) Cultured hippocampal neurons at 18 DIV pretreated with IBMX and forskolin were treated with Acad-EC (10 μg/ml) for 30 min followed by immunostaining (left) for arcadlin (green) and phospho-p38 MAPK (red); corresponding immunoblot shown to the right.

(F) Reconstitution of the arcadlin-TAO2β-p38 MAPK pathway in HEK293T cells transfected as described. Cells in (C) were pretreated with 10 μM SB203580. Cells were treated with Acad-EC for 30 min and immunostained for phospho-p38 MAPK.

(G) Quantification of surface arcadlin level by biotinylation method in HEK293T cells transfected and treated as indicated. Densitometric quantification from five separate experiments is summarized in histogram (mean ± SEM).

**$p < 0.01$. Scale bars, 10 μm.

activity of TAO2α and -β that resides in their common catalytic domains is sufficient for the phosphorylation and activation of p38 MAPK. The endocytosis of arcadlin, however, depends exclusively on TAO2β, suggesting that the unique carboxy-terminal domain of TAO2β is required for the endocytosis of the arcadlin protocadherin.

### A TAO2β-p38 MAPK Feed-Back Loop Mediates the Endocytosis of Arcadlin

We next investigated the requirement of p38 MAPK for the endocytosis of arcadlin. We found that SB203580, a p38 MAPK inhibitor, blocked the endocytosis of arcadlin (Figure 5G, compare lanes 2 and 3). This suggested that a feed-back loop, in which p38 MAPK regulates the endocytosis of arcadlin, might exist. We first postulated that arcadlin itself was a direct substrate of p38 MAPK. However, arcadlin was not phosphorylated by p38 MAPK (data not shown). We then tested whether p38 MAPK phosphorylates TAO2β. Because the experiments above indicated that the function of TAO2β responsible for the endocytosis of arcadlin resided in the carboxy-terminal domain, the unique carboxy-terminal region (751–1056) of TAO2β was fused to glutathione S-transferase (GST) and subjected to an in vitro kinase reaction with purified p38 MAPK. GST-TAO2β (751–1056) was indeed phosphorylated by activated p38 MAPK (Figure 6A, lane 2). Within this region, there were two sites encoding a serine preceded by a proline in positions 951 and 1010 as possible substrate sites for MAPK family members (Figure 6B; Kyriakis and Avruch, 2001), but their mutation into phosphorylation-resistant alanines did not affect the incorporation of $^{32}P$ (Figure 6A, lane 3 and data not shown). A detailed deletion mutant analysis (data not shown) then revealed that the main target of p38 MAPK was localized within the region between positions 1036 and 1056 (Figure 6B). We generated Ser to Ala point mutations on positions 1038, 1040, 1042, and 1045 and found that incorporation of $^{32}P$ diminished in TAO2βS1038A, indicating that Ser1038 is the main target of p38 MAPK (Figures 6A and 6B, lane 4).

We next investigated whether phosphorylation of Ser1038 was required for the endocytosis of arcadlin. Cells expressing TAO2βS951A, used here as a control, exhibited normal endocytosis of arcadlin, whereas the phosphorylation-resistant TAO2βS1038A remained in the surface after addition of Acad-EC protein (Figure 6C, lanes 1–4; see Figure 6D for quantification). Time-lapse images of HEK293T cells expressing arcadlin-EYFP and TAO2βS1038A-ECFP or control TAO2βS951A-ECFP confirmed that TAO2βS1038A fails to induce the endocytosis of arcadlin in living cells (Figure 6E).

These results indicate that the p38 MAPK that is activated by the arcadlin-TAO2β-MEK3 signaling pathway in turn phosphorylates TAO2β on Ser1038, resulting in the formation of a feed-back signaling loop. Phosphorylation of Ser1038 of TAO2β seems to be essential to activate the endocytic machinery following homophilic interaction of arcadlin. Thus, it appears we have identified a molecular pathway for protocadherin-mediated endocytosis.

### The Arcadlin-TAO2β-p38 MAPK Pathway Regulates N-Cadherin Endocytosis

Finally, we tested whether the arcadlin-induced internalization of N-cadherin is mediated by the arcadlin-TAO2β-p38 MAPK molecular pathway defined above. The quantification of neuronal surface proteins by biotinylation showed that treatment with Acad-EC caused the reduction in surface arcadlin/N-cadherin levels in neurons (Figure 7A; see Figure 7B for quantification). This reduction was inhibited by SB203580, suggesting that the internalization was mediated by the p38 MAPK pathway (Figures 7A and 7B). Although arcadlin also binds to cadherin-11 (see Figure 1K), there was no significant endocytosis of cadherin-11 upon the treatment with Acad-EC (Figures 7C and 7D). It seems that arcadlin is targeted to multiple species of classical cadherins, but not all of them undergo the endocytosis through this pathway. Individual classical cadherins might code for distinct subsets of synapses.

Similar results were obtained in the microscopic quantification of N-cadherin internalization. A 28.3% ± 2.7% decrease in the mean intensity of total surface N-cadherin in the Acad-EC treatment group (30 min) relative to control was observed. The decrease in the surface N-cadherin mean intensity was observed in both the synaptic and extrasynaptic populations (Figure 7E). In *acad*$^{-/-}$ neurons, there was no significant change in the mean intensity of total surface N-cadherin in the Acad-EC treatment group relative to control (Figure 7E).

In HEK293T cells cotransfected with *arcadlin*, *N-cadherin*, and *tao2β*, addition of Acad-EC protein also triggered endocytosis (Figure S3). Arcadlin and N-cadherin were cointernalized in the presence of TAO2β but were retained on the plasma membrane in its absence (Figure S3). Taken together, these data indicate that the internalization of N-cadherin is mediated by the arcadlin-TAO2β-p38 MAPK molecular pathway and triggered by homophilic interactions between arcadlin protocadherin extracellular domains.

### Arcadlin Mutation Increases Dendritic Spine Density

What is the consequence of the arcadlin-induced internalization of N-cadherin in the dendritic spine membrane? To address this question, we examined the morphology and the number of spines of hippocampal neurons. Cultured hippocampal neurons derived from *acad*$^{-/-}$ mice protruded a significantly larger number of spines than wild-type neurons (Figure 8B). This phenotype was rescued by the transfection of *arcadlin* cDNA (Figures 8A and 8B and Figure S4A). The rescuing effect was more prominent where the axons of transfected neurons were attached to the transfected dendrites (Figure 8A, square bracket). The other splice variant *arcadlin-L* did not recover the spine

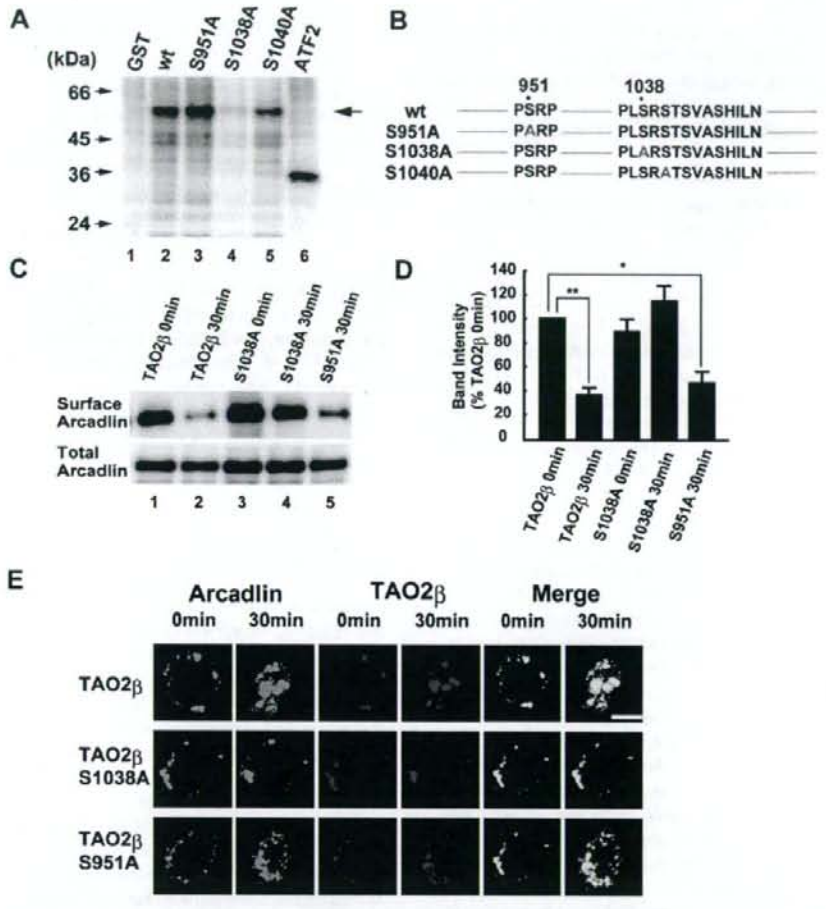


**Figure 6. Feed-Back Phosphorylation of TAO2β at Ser1038 by p38 MAPK Is Essential for the Endocytosis of Arcadlin**

(A) GST-TAO2β, -TAO2βS951A, -TAO2βS1038A, or -TAO2βS1040A were incubated with activated p38 MAPK and [γ-$^{32}$P]ATP and subjected to SDS-PAGE followed by autoradiography. The activated p38 MAPK was prepared by immunoprecipitation from Acad-EC-treated HEK293T cells transfected with *arcadlin*, *tao2β*, *MEK3*, and *p38 MAPK*. Arrow indicates $^{32}$P-incorporated GST-TAO2β mutant proteins. ATF2, a positive control.

(B) Mutations of TAO2β examined as substrates of p38 MAPK.

(C) Surface-biotinylation assay of arcadlin in HEK293T cells transfected with *arcadlin*, *MEK3*, *p38 MAPK*, and *tao2β* (or *tao2βS1038A* or *tao2βS951A*) before and 30 min after the addition of Acad-EC into culture medium.

(D) Quantification histogram of three independent results of (C) (mean ± SEM).

(E) Time-lapse confocal images of live cells expressing arcadlin-EYFP and TAO2β-ECFP (top), phosphorylation-resistant TAO2βS1038A-ECFP (middle), or control TAO2βS951A-ECFP (bottom) before and 30 min after Acad-EC treatment.

*$p < 0.05$, **$p < 0.01$. Scale bar, 10 μm.

number (Figures 8A and 8B and Figure S4A), indicating that only arcadlin, not arcadlin-L, regulates spine density.

We then asked whether the N-cadherin endocytosis caused the arcadlin-induced change in spine density. There are several studies showing the relationship between N-cadherin activity and spine number. The spine number of *N-cadherin* KO neurons is maintained (Jungling et al., 2006; Kadowaki et al., 2007); a sustained period of N-cadherin loss in these neurons might allow other synaptic cell adhesion molecules to compensate for N-cadherin. In contrast, spine number is suppressed in neurons whose N-cadherin is knocked down by RNAi techniques (Saglietti et al., 2007). Consistently, an expression of a dominant-negative form of N-cadherin reduces the number of synaptic puncta (Togashi et al., 2002). In the present study, the spine density of *acad*$^{-/-}$ neurons was reduced by siRNA knockdown of N-cadherin (Figures 8C and 8D and Figure S4B). Moreover, a similar